

In presenting the dissertation as a partial fulfillment of the requirements for an advanced degree from the Georgia Institute of Technology, I agree that the Library of the Institute shall make it available for inspection and circulation in accordance with its regulations governing materials of this type. I agree that permission to copy from, or to publish from, this dissertation may be granted by the professor under whose direction it was written, or, in his absence, by the Dean of the Graduate Division when such copying or publication is solely for scholarly purposes and does not involve potential financial gain. It is understood that any copying from, or publication of, this dissertation which involves potential financial gain will not be allowed without written permission.

7/25/68

A STUDY OF IMPACT MOTION BASED ON RHEOLOGICAL MODELING

A THESIS

Presented to

The Faculty of the Division of Graduate

Studies and Research

by

William Edward Pugh, III

In Partial Fulfillment

of the Requirements for the Degree

Master of Science

in the School of Mechanical Engineering

Georgia Institute of Technology

July, 1971

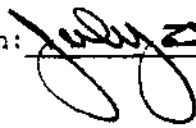
A STUDY OF IMPACT MOTION BASED ON RHEOLOGICAL MODELING

Approved:



Chairman

Date approved by Chairman:

 July 20, 1971

ACKNOWLEDGMENTS

The author is indebted to his advisor, Dr. Joseph R. Baumgarten, for suggesting the thesis topic and for giving continued enthusiasm and help in its execution. The members of the reading committee, Drs. Ward O. Winer and Charles E. Stoneking, provided useful suggestions and timely comments which were helpful in preparing the final draft.

Appreciation is also expressed to the National Aeronautics and Space Administration (NASA) which funded the author's study and to Dr. Stephen L. Dickerson, the NASA Design Coordinator, for constant guidance and continuing interest in the author's graduate program.

Special thanks are also due the staff of the School of Mechanical Engineering for their assistance in this endeavor and to the author's colleagues for helpful discussions on various phases of the research.

The author is especially grateful to his parents who wisely encouraged his scientific interests at an early age and who made many sacrifices to further his education, as well as to his brother whom he recognizes as his first engineering colleague.

Finally the author thanks his wife for her constant encouragement and for the many personal ambitions she has given up or postponed in the interest of his education.

TABLE OF CONTENTS

	Page
ACKNOWLEDGMENTS.	ii
LIST OF TABLES	v
LIST OF ILLUSTRATIONS.	vi
LIST OF PRINCIPAL NOMENCLATURE	viii
SUMMARY.	xi
Chapter	
I. INTRODUCTION.	1
II. ANALYTICAL INVESTIGATION.	7
Introduction	
Free Motion	
Motion During Impact	
Kelvin-Voigt Model	
Poynting-Thomson Model	
Impacting Kelvin-Voigt Penduli	
Introduction	
Altered Kelvin-Voigt Model	
Free Motion	
Determination of System Parameters	
Impacting Poynting-Thomson Penduli	
III. EXPERIMENTAL APPARATUS AND PROCEDURE.	23
Apparatus	
Mechanical Test Device	
Instrumentation	
Experimental Procedure	
Set Up and Calibration	
Typical Run Procedure	
Reduction of Data	
IV. CORRELATION OF EXPERIMENTAL AND THEORETICAL RESULTS . . .	36
Generation of the Theoretical Response Curves	
Comparison of Theoretical and Experimental Response	
Comparison of Theoretical Solutions Using	
Slightly Varied Parameters	

Chapter	Page
V. CONCLUSIONS AND RECOMMENDATIONS	45
The Experimental Device	
Rheological Models	
APPENDIX	
A. DERIVATION OF POYNTING-THOMSON EQUATIONS.	52
B. DESIGN OF ELECTROMAGNETS.	59
C. DRAWINGS FOR SELECTED EXPERIMENTAL PARTS.	61
D. DIGITAL COMPUTER PROGRAM CALIBR	68
E. DIGITAL COMPUTER PROGRAM PENDUL	70
F. ANALYSIS OF SUPPORT CABLE ORIGINATED FORCING FUNCTION . . .	74
BIBLIOGRAPHY	84

LIST OF TABLES

Table		Page
1.	Experimental Equipment.	28
2.	Deviation of Theoretical Response from Experimental Response.	37
3.	Values of K Versus $\sqrt{\xi}$ for the Bars Tested	42
4.	Comparison of Predicted and Calculated Theoretical Response for the 0.405-Inch Initial Displacement Case . . .	44

LIST OF ILLUSTRATIONS

Figure		Page
1.	Rheological Models Including Only Viscous Dissipation Elements.	4
2.	Rheological Models Including Coulomb Dissipation Elements.	5
3.	Nomenclature for the Ballistic Pendulum	8
4.	Kelvin-Voigt Model.	10
5.	Poynting-Thomson Model.	10
6.	Nomenclature for Rebounds	13
7.	Synthesis of Equation 20 from Equation 19	15
8.	Experimental Test Device.	24
9.	Photocell Biasing Circuit	25
10.	Displacement Transducers.	25
11.	Contact Time Instrumentation.	26
12.	Magnet Release Circuit.	27
13.	Plot of Oscilloscope Trace and Pendulum Displacement.	31
14.	Photocell Calibration Curve	32
15.	Enumeration of Rebounds from Oscillograph	34
16.	Response for 0.598-Inch Initial Displacement.	40
17.	Response for 0.713-Inch Initial Displacement.	40
18.	Response for 1.519-Inch Initial Displacement.	40
19.	Measured Contact Time Versus Initial Displacement	41
20.	C Versus \sqrt{E} for the Bars Tested	43
21.	Electromagnet	60

Figure	Page
22. Magnet Holder	62
23. Support Wire Guide.	63
24. Wire Guide Support Bracket.	64
25. Test Bar Support Rings.	65
26. Steel Mass.	66
27. Wooden Frame.	67
28. Support Wire Nomenclature	75
29. \bar{y} -z Plane	76

LIST OF PRINCIPAL NOMENCLATURE*

A	a parameter
\bar{A}	a parameter
a	a parameter
B	a parameter
b	a parameter
C	viscous damping coefficient, a constant
C_c	critical viscous damping coefficient
D	a parameter
d	diameter, a parameter
E	a parameter
e	base of the natural logarithms
F	force
g	acceleration due to gravity
H	force component
i	integer index, $\sqrt{-1}$
K	linear spring constant
l	chord length
L	pendulus length

*The symbols listed above are used throughout the thesis with the meaning indicated. Where multiple definitions are given, the usage is obvious from the context. Units of measurement, where necessary, are specified in the thesis body. The symbols used in the digital computer programs may vary slightly from those presented here due to the limited character set. The meanings, if not obvious, are defined in the programs themselves.

\tilde{L}	a parameter
M	mass
m	mass
N	integer index
NI	number of ampere-turns
n	integer index
p	a parameter
r	radius
S	arc length
s	the Laplace variable
T	kinetic energy, tension, a function
t	time
U	potential energy
V	force component
v	velocity
W	weight of pendulus mass
X	horizontal displacement
x	rectangular coordinate
\bar{x}	rectangular coordinate
Y	vertical displacement, a function
y	rectangular coordinate
\bar{y}	rectangular coordinate
z	rectangular coordinate
α	angular measure
β	magnetic flux density

γ	angular measure, a parameter
ζ	damping ratio
θ	angular displacement
λ	a parameter
μ	permeability
ξ	coefficient of restitution
$\frac{1}{2}$	ratio of impact energies
π	3.14159
ρ	mass density, a parameter
$\bar{\rho}$	mass per unit length
τ_c	contact duration
τ_r	rebound duration
ϕ	phase angle
ω	rotational frequency, a parameter
ω_d	damped natural frequency
ω_n	natural frequency

SUMMARY

It is the objective of this research to determine whether rheological models could be used to describe the macroscopic response of viscoelastic bodies in impact. The applicability of 12 models is discussed with primary emphasis placed on the Kelvin-Voigt model. An analysis of pendulus impact which results in closed form expressions for the parameters of this model is made assuming the rebounds to be conservative and a FORTRAN program which implements the analysis is presented.

An experimental device, which consists of the ballistic suspension of two masses which touch in the position of static equilibrium with null normal force, was designed and built to collect data on the behavior of materials in impact. With this equipment rebound histories were recorded for various initial impacting velocities and the experimental responses compared with the theoretical. From these comparisons recommendations on improvements in experimental technique and analytical development are made.

It was found that the parameters of the Kelvin-Voigt model vary with impacting velocity in much the same way as does the coefficient of restitution, and it is shown that the response obtained from the Kelvin-Voigt formulation is identical to that which would attain had the coefficient of restitution been used. Some allowable design expedients with regard to the Kelvin-Voigt model are suggested but the results indicate

that a better quantitative understanding of the nature of energy dissipation in impact will have to be developed before impact responses can be predicted from material properties alone.

CHAPTER I

INTRODUCTION

It was the objective of this research to determine whether rheological models could be used to describe the macroscopic response of visco-elastic bodies in impact. In particular it was sought to describe the low frequency high amplitude motions of rebound rather than the high frequency low amplitude oscillations of stress wave propagation and ringing.

The ability to define the rebound motion of impacting bodies has practical significance in several areas of mechanical design and is of particular value in high-speed machinery involving positive action cams, mechanical indexing or impact printing.

Historically rebound has been treated by first writing the conservation of momentum relations for perfectly elastic collisions and then scaling the resultant departing velocities by a factor known as the coefficient of restitution (1). The idea may be expressed mathematically as

$$\sum_i m_i \hat{v}_{i1} = \sum_i \epsilon m_i \hat{v}_{i2} \quad (1)$$

where v_{i1} is the initial (approaching) velocity of mass i (m_i) and v_{i2} is the final (departing) velocity of m_i and so on. The coefficient

of restitution ξ is the ratio of departing and approaching velocities and in equation 1 is implied to be identical for all of the bodies.

For bodies rebounding in a conservative potential field, the ratio of rebound heights, h_2/h_1 , which may be thought of as the mechanical efficiency of the collisions, is significant. Realizing that this is the ratio of total system energies before and after impact and equating it to the ratio of the maximum kinetic energies results in

$$\xi = h_2/h_1 = U_2/U_1 = T_2/T_1 = V_2^2/V_1^2 = \xi^2 \quad (2)$$

The coefficient of restitution ξ is dependent upon the materials of the bodies, their sizes and shapes, and upon the relative impacting velocities. In application, the coefficients of restitution must be found experimentally for two particular bodies impacting at various velocities. However, for some common shapes in common materials, ξ has been catalogued for varying impact velocities (2).

Rheological models, which are various arrangements of lumped parameter mechanical elements, have been used to describe creep deformation and, in impact, to analyze stress wave propagation (3). Because rheological models contain energy dissipation terms, they are capable of predicting rebound velocities directly, without the use of a coefficient of restitution. However, these models contain several other parameters which must be determined experimentally.

Rheological models result in equations of motion which involve impacting velocities only as boundary conditions. Thus it may be that

the parameters in these models depend only on the materials, sizes, and shapes of the impacting bodies, so long as the range of impacting velocities is such that no basic changes in the primary energy dissipation phenomena occur.

A survey of rheological models for visco-elastic materials was made. They may be separated into two groups, those models containing only viscous dissipation terms and those containing Coloumb dissipation terms. The configurations are shown in Figures 1 and 2.

As the force produced in a dashpot is proportional to the relative velocity of its parts, such a device cannot support a static load. Therefore, any model which does not incorporate a displacement proportional spring in parallel with each dashpot is incapable of resisting a static load and is inappropriate for modeling steel or most other solids.

Coloumb elements cannot support loads greater than some maximum F_0 . When forces greater than F_0 are applied, the deformation is accelerated by a force $F - F_0$. This type of deformation may be typical of brittle fracture but is not thought to be typical of energy dissipation in low velocity impact (4). Therefore, models not incorporating a displacement proportional spring in parallel with each Coloumb dissipation element are appropriate for modeling ductile materials.

Referring to Figures 1 and 2 and eliminating models involving Coloumb friction elements and/or viscous dampers not paralleled by a displacement proportional spring, the rheological models which show promise in modeling low velocity impact are the Hook, Kelvin-Voigt and Poynting-Thomson Models, Figures 1 (A), (C), (E), respectively.

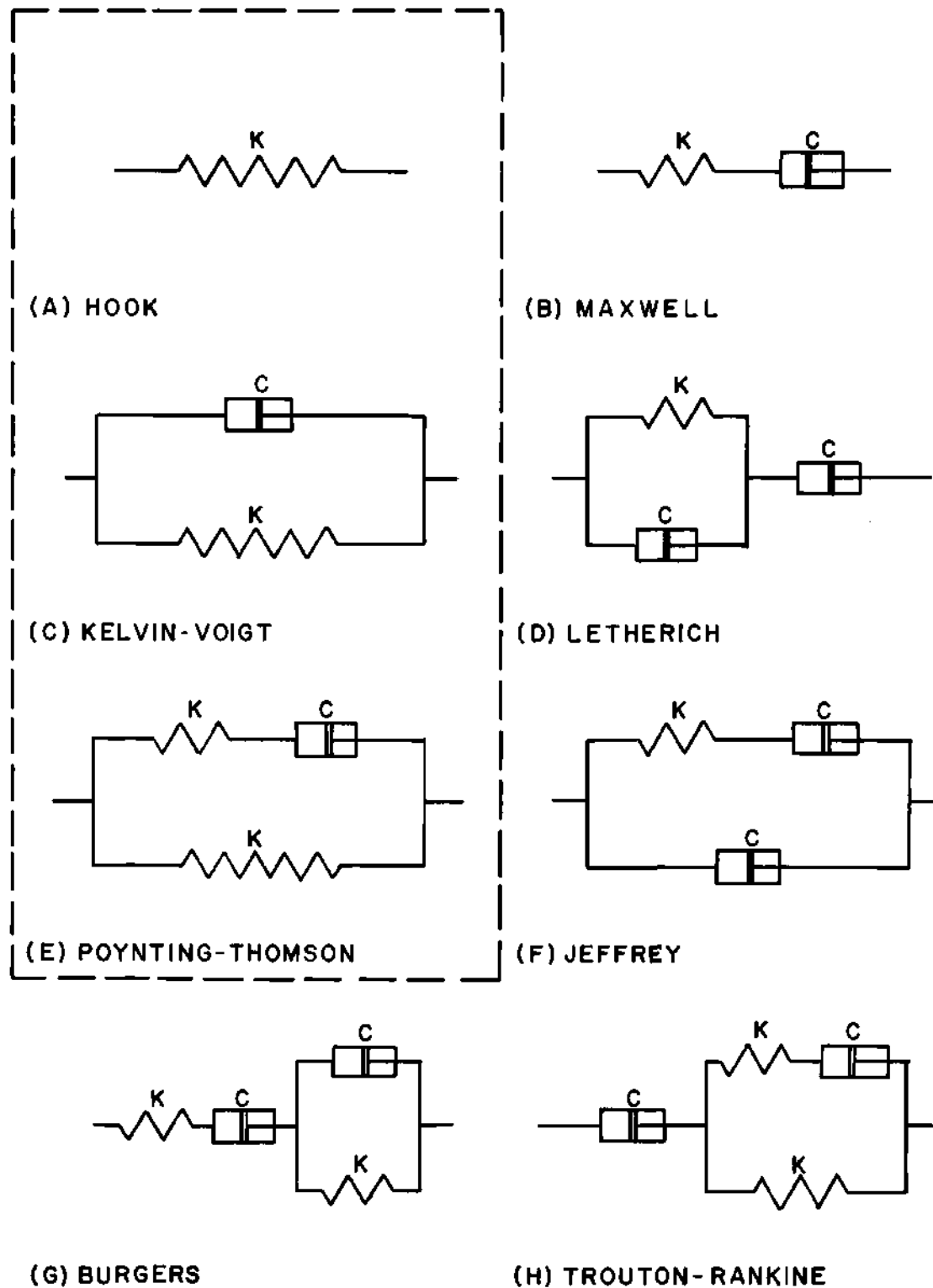
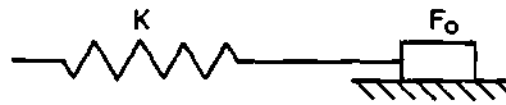
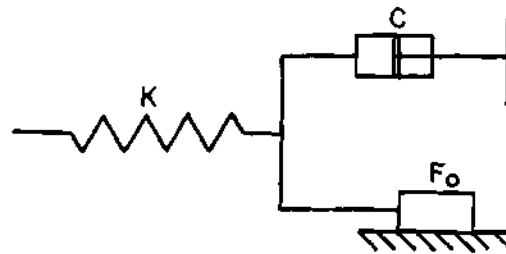


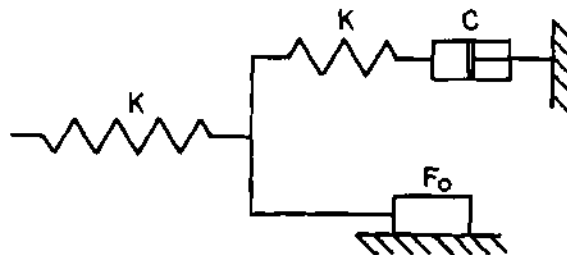
Figure 1. Rheological Models Including Only Viscous Dissipation Elements



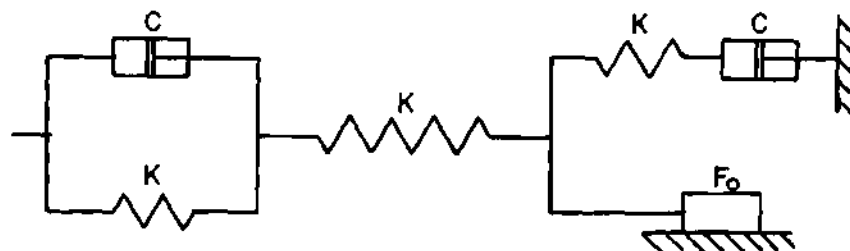
(A) PRANDTL



(B) BINGHAM



(C) SCHWEDOFF



(D) SCHOFIELD-SCOTT-BLAIR

Figure 2. Rheological Models Including Coloumb Dissipation Elements

The Hookian model has been widely used and describes perfectly elastic impact ($C=0$, $\xi=1$). In this thesis the Kelvin-Voigt and Poynting-Thomson models received further study.

CHAPTER II

ANALYTICAL INVESTIGATION

The experimental device, which consists of the ballistic suspension of two identical masses which touch in the position of static equilibrium with a null normal force, is such that two motion conditions exist. While the masses are out of contact the motion is that of a freely oscillating ballistic pendulum; during contact the bodies act as mass-spring-damper systems with one end fixed.

It is advantageous to make the study as independent of the peculiarities of the experimental device as possible. Therefore the impacting velocities are used as initial conditions for the rheological models. Also the measured parameters, contact time and maximum rebound potential energy (measured as maximum rebound displacement), are not unique to the experimental device.

The analysis is made by first studying the free motion and then analyzing the rheological impact model. The two solutions are then combined into an expression valid for several rebounds. It has been assumed that all energy dissipation occurs during contact and therefore that the rebounds are conservative.

Free Motion

The ballistic pendulum, Figure 3, has the following equation of motion for small displacements

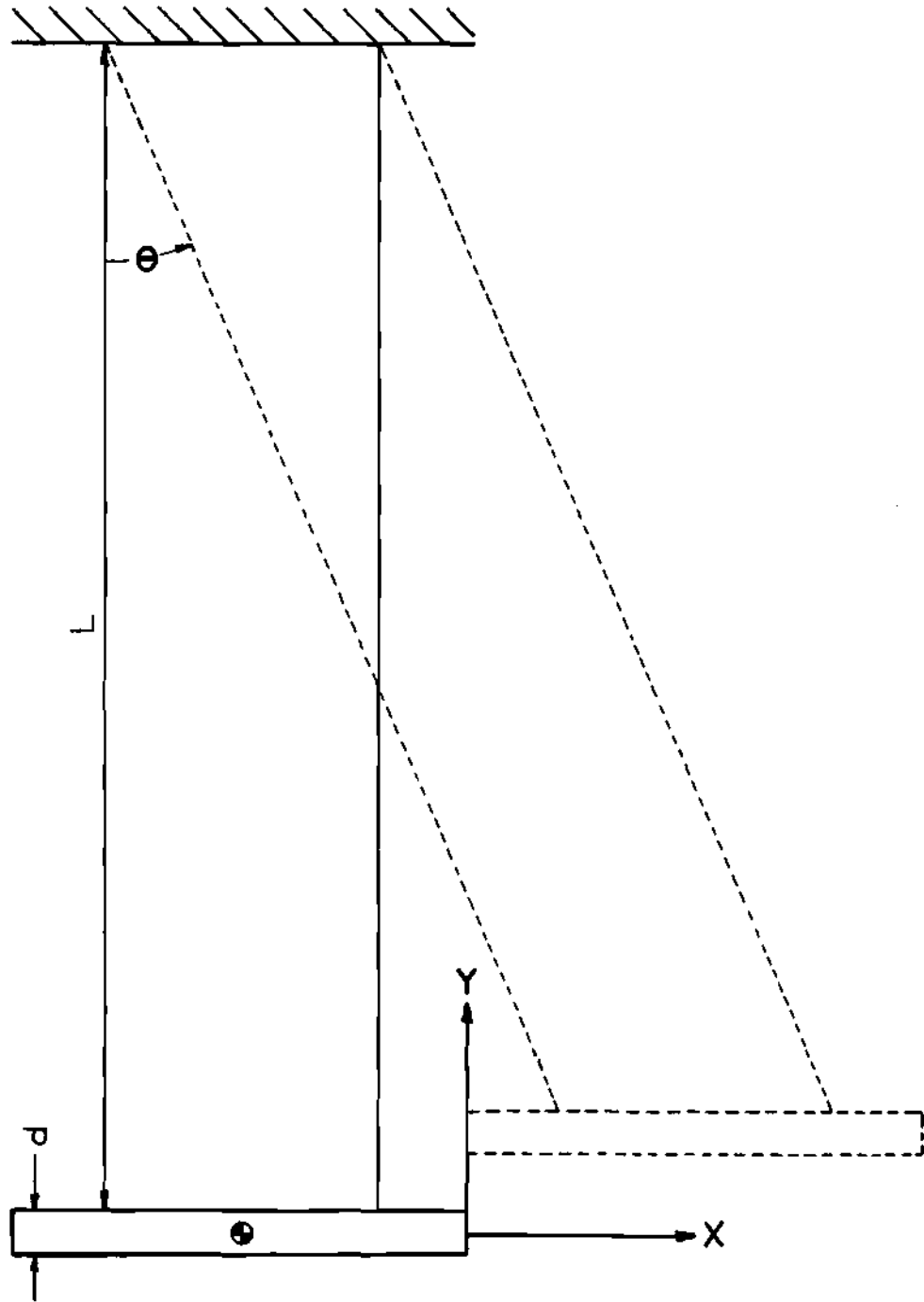


Figure 3. Nomenclature for the Ballistic Pendulum

$$\ddot{\theta} + g/L = 0 \quad (3)$$

The solutions to equation 3 are

$$\theta = \theta_0 \cos \sqrt{g/L} t \quad \text{for} \quad \theta(0) = \theta_0, \dot{\theta}(0) = 0 \quad (4)$$

and

$$\theta = \dot{\theta}_0 \sqrt{L/g} \sin \sqrt{g/L} t \quad \text{for} \quad \theta(0) = 0, \dot{\theta}(0) = \dot{\theta}_0 \quad (5)$$

Notice from the figure that

$$X = L \sin \theta \quad (6)$$

and

$$Y = L(1 - \cos \theta) \quad (7)$$

Motion During Impact

Kelvin-Voigt Model

The Kelvin-Voigt Model, Figure 4, has, upon balancing forces, the equation of motion

$$\ddot{X} + \dot{X}C/M + XK/M = 0 \quad (8)$$

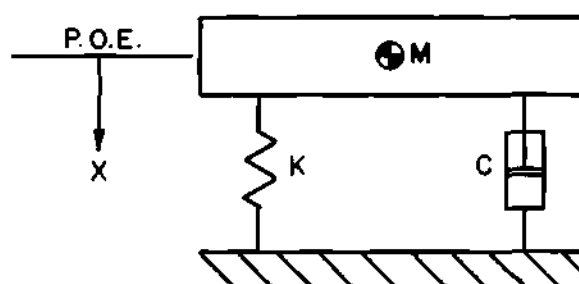


Figure 4. Kelvin-Voigt Model

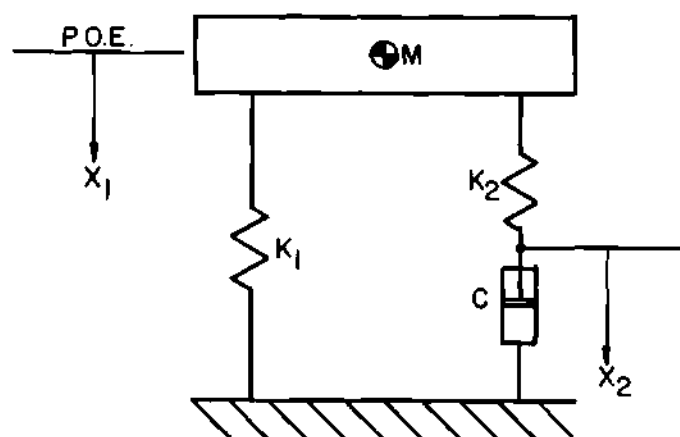


Figure 5. Poynting-Thomson Model

This equation has, for the specified initial conditions, the solution

$$x = (1/\omega_d) \dot{x}_0 e^{-\zeta \omega_n t} \sin \omega_d t \quad \text{for} \quad x(0) = 0, \dot{x}(0) = \dot{x}_0 \quad (9)$$

where

$$\omega_n = \sqrt{K/M} \quad \zeta = C/C_c = C/2M\omega_n \quad \omega_d = \omega_n \sqrt{1-\zeta^2} \quad (10)$$

The velocity of the center of mass during contact is given by the first time derivative of equation 10 and may be written as

$$\dot{x} = \dot{x}_0 \sqrt{1-\zeta^2} e^{-\zeta \omega_n t} \cos(\omega_d t + \phi) \quad (11)$$

where

$$\phi = \arctan(\zeta/\sqrt{1-\zeta^2}) \quad (12)$$

Poynting-Thomson Model

Balancing forces on the Poynting-Thomson model, Figure 5, results in the following equations of motion

$$\ddot{x}_1 + (K_1 + K_2)x_1/M - K_2x_2/M = 0 \quad (13)$$

$$C\dot{X}_2 - K_1 X_1 + K_2 X_2 = 0 \quad (14)$$

It may be shown (Appendix A) that equations 13 and 14 have solutions of the form

$$X_1(t) = \gamma_1 e^{-\rho_1 t} + \gamma_2 e^{-\rho_2 t} \sin(\omega t + \phi_1) \quad (15)$$

$$X_2(t) = \gamma_3 e^{-\rho_1 t} + \gamma_4 e^{-\rho_2 t} \sin(\omega t + \phi_2)$$

or

$$X_1(t) = \gamma_5 e^{-\rho_3 t} (t + \gamma_6 t^2) \quad (16)$$

$$X_2(t) = \gamma_7 t^2 e^{-\rho_3 t}$$

or

$$X_1(t) = \gamma_8 e^{-\rho_4 t} + (\gamma_9 t + \gamma_{10}) e^{-\rho_5 t} \quad (17)$$

$$X_2(t) = \gamma_{11} e^{-\rho_4 t} + (\gamma_{12} t - 1) e^{-\rho_5 t}$$

or

$$X_1(t) = \gamma_{13} e^{-\rho_6 t} + \gamma_{14} e^{-\rho_7 t} + \gamma_{15} e^{-\rho_8 t} \quad (18)$$

$$X_2(t) = \gamma_{16} e^{-\rho_6 t} + \gamma_{17} e^{-\rho_7 t} + \gamma_{18} e^{-\rho_8 t}$$

Positive displacements are away from the position of static equilibrium (to the right in the figure) and time is increasing downward. The rebounds and impacts are numbered as indicated. $N=0$ being the initial positive displacement. Impact 1 precedes rebound 1 and so on.

From equation 9 for the Kelvin-Voigt model, rewritten below,

$$X = (1/\omega_d) \dot{x}_0 e^{-\zeta \omega_n t} \sin \omega_d t \quad (19)$$

it is seen that the duration of contact is constant for a fixed set of parameters K , C , and M , and is equal to the half period $\tau_c = \pi/\omega_d$. From equations 4 and 5 for the ballistic pendulum, it is known that the duration of any rebound is constant for fixed pendulum length L and gravitational constant g and is equal to the half period $\tau_p = \pi\sqrt{L/g}$. The time from initial release to first contact is obviously $0.5 \tau_p = \pi\sqrt{L/g}/2$.

Altered Kelvin-Voigt Model

Equation 19 must be altered to reflect the facts that only negative (compressive) displacements occur in impact and that half cycles of contact are separated by rebounds of duration τ_p . As depicted in Figure 7, the altered form of equation 19 is

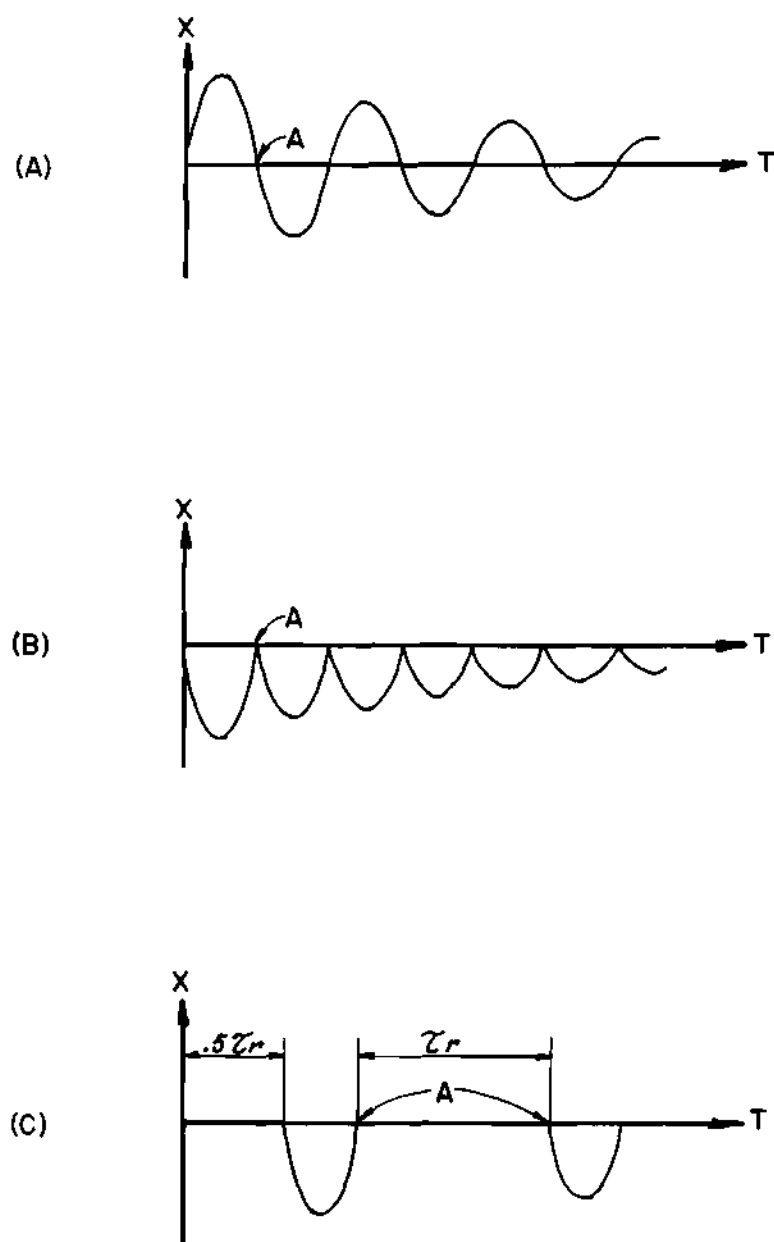


Figure 7. Synthesis of Equation 20 from Equation 19

$$X = -\left|(1/\omega_d)\dot{X}_0 e^{-\zeta\omega_n[t - (N-1/2)\tau_r]} \sin\omega_d[t - (N-1/2)\tau_r]\right| \quad (20)$$

for $(N-1)\tau_c + (N-1/2)\tau_r \leq t \leq N\tau_c + (N-1/2)\tau_r$.

Further justification of equation 20 is made by noting that for an ideal pendulum in a conservative field, the separating velocity of impact N is of the same magnitude as the approaching velocity of impact $N+1$ (see Figure 6). Therefore points "A" in Figure 7 have the same displacement (zero) and the same velocity magnitude. Thus if alternate impacts in Figure 7 (C) were reflected about the abscissa and then compressed to remove gaps τ_r , curve 7 (A) would result and equation 19 would apply.

Free Motion

From the initial position the displacement equation of the specimen is

$$\theta = \theta_0 \cos\sqrt{g/L} t \quad (21)$$

It can be shown that for small displacements the horizontal component of the motion, X , is given by

$$X = L\theta_0 \cos\sqrt{g/L} t \quad (22)$$

But $X_0 = L\theta_0$, thus

$$X = X_0 \cos \sqrt{g/L} t \quad (23)$$

The free motion after impact is given by equation 11 modified to account for the fact that the initial condition $\dot{\theta}_0$ is different for each rebound and to properly account for the separation of half cycles.

$$\theta = \dot{\theta}_{N_0} \sqrt{L/g} \sin \sqrt{g/L} [t - N\tau_c - (N - 1/2)\tau_r] \quad (24)$$

for $N\tau_c + (N-1/2)\tau_r \leq t \leq N\tau_c + (N+1/2)\tau_r$ $N=1,2,3,\dots$

Following the same type of argument as made for the free motion before impact, we write over the same range as equation 24

$$X = \dot{X}_{N_0} \sqrt{L/g} \sin \sqrt{g/L} [t - N\tau_c - (N - 1/2)\tau_r] \quad (25)$$

where $\dot{X}_{N_0} = L\dot{\theta}_{N_0}$ is the initial departing velocity for the N th rebound.

Equation 20 may be written

$$X = (-1)^N (\dot{X}_0/\omega_d) e^{-\xi\omega_n[t - (N - 1/2)\tau_r]} \sin \omega_d [t - (N - 1/2)\tau_r] \quad (26)$$

Differentiating this form of equation 20 once with respect to time yields

$$\dot{X} = (-1)^N (\dot{X}_0 / \sqrt{1 - \xi^2}) e^{-\xi \omega_n [t - (N - 1/2)\tau_r]} \cos\{\omega_d [t - (N - 1/2)\tau_r] + \phi\} \quad (27)$$

where

$$\phi = \arctan(\xi / \sqrt{1 - \xi^2}) \quad (28)$$

\dot{X}_{N_0} in equation 25 is given by equation 27 evaluated at $t = (N - 1/2)\tau_r + N\tau_c$, thus

$$\dot{X}_{N_0} = (-1)^N (\dot{X}_0 / \sqrt{1 - \xi^2}) e^{-\xi \omega_n N \tau_c} \cos(\omega_d N \tau_c + \phi) \quad (29)$$

Finally, equation 25 may be written

$$X = [(-1)^N (\dot{X}_0 \sqrt{L/g} / \sqrt{1 - \xi^2}) e^{-\xi \omega_n N \tau_c} \cos(N\pi + \phi)] \sin \sqrt{g/L} [t - N\tau_c - (N - 1/2)\tau_r] \quad (30)$$

for $(N - 1/2)\tau_r + N\tau_c \leq t \leq (N + 1/2)\tau_r + N\tau_c$ $N = 1, 2, 3, \dots$, since

$$\tau_c = \pi / \omega_d.$$

Determination of System Parameters

The parameters K , C and M must be found experimentally. It is expeditious to measure M directly. Values for K and C must then be determined. This can be done if the period of contact τ_c of any impact,

the maximum rebound displacement of any rebound and the initial displacement are measured.

Referring to Figure 6, it may be seen that at $X = 0$ (the position of static equilibrium, P.O.E.) and $t = N\tau_c + (N - 1/2)\tau_r$ the kinetic energy $T = 1/2 M\dot{X}^2$ is identically equal to the potential energy U at $t = N\tau_c + N\tau_r$.

The maximum kinetic energy in the N th rebound is found by substituting equation 29 into the expression for kinetic energy.

$$T_{Nmax} = (M/2)[(-1)^N(\dot{X}_0/\sqrt{1-\zeta^2})e^{-\zeta\omega_n N\tau_c} \cos(\omega_d N\tau_c + \phi)]^2 \quad (31)$$

Recalling that $\tau_c = \pi/\omega_d$ and $\tan \phi = \zeta/\sqrt{1-\zeta^2}$, equation 31 becomes, upon simplification

$$T_{Nmax} = (M\dot{X}_0^2/2)e^{-2N\pi\zeta/\sqrt{1-\zeta^2}} \quad (32)$$

The maximum potential energy in the N th rebound is given by

$$U_{Nmax} = MgL[1 - \cos(X_{Nmax}/L)] \quad (33)$$

Equating equations 32 and 33, simplifying and taking the natural logarithm of both sides of the expression results in

$$-2N\pi\zeta/\sqrt{1-\zeta^2} = \ln\{(2gL/\dot{X}_0^2)[1 - \cos(X_{N\max}/L)]\} = \bar{L} \quad (34)$$

A new parameter \bar{L} involving $X_{N\max}$ and \dot{X}_0 has thus been defined.

For experimental convenience recall that $\dot{X}_0 = X_0\sqrt{g/L}$. \bar{L} may then be written as

$$\bar{L} = \ln\{(2L^2/X_0^2)[1 - \cos(X_{N\max}/L)]\} \quad (35)$$

Thus \bar{L} can be found from an N th cycle using measurable quantities L , initial displacement X_0 , and rebound height $X_{N\max}$. Solving equation 34 for ζ in terms of \bar{L} yields

$$\zeta = \sqrt{\bar{L}^2/(\bar{L}^2 + 4N^2\pi^2)} \quad (36)$$

which is an expression for the damping ratio in terms of measurable quantities at the N th rebound.

Recalling that $\tau_c = \pi/\omega_d$ and $\omega_d = \sqrt{K(1-\zeta^2)}/M$ we find

$$K = M\pi^2/[\tau_c^2(1-\zeta^2)] \quad (37)$$

Hence the spring constant K may be computed from the known mass M , the observed contact time τ_c , and the damping ratio calculated from equation 36.

Finally from the definition of ζ

$$C = 25\sqrt{KM} \quad (38)$$

Thus the system parameters may be determined.

Equation 34 may be verified by equating the change in maximum potential energies in the N th and $(N-1)$ st rebounds to the energy dissipated in the dashpot during the N th impact.

$$Mg(Y_{(N-1)max} - Y_{Nmax}) = \int_{(N-1)\tau_c}^{N\tau_c + (N-1/2)\tau_r} C\dot{X}^2 dt \quad (39)$$

(Note that $C\dot{X}^2 dt = C\dot{X}dX$.)

Impacting Poynting-Thomson Penduli

As indicated in the section on the Poynting-Thomson model, the displacement equations which are solutions to the differential equations of motion for this model have different forms depending on the values of the parameters K_1 , K_2 , C and M . Following the approach of the previous section, one would choose one of the forms of the solution, say solution A, and use it to describe initial conditions for each rebound of the freely oscillating pendulum. From the resulting equation one would seek expressions for the parameters of the model in terms of measurable quantities, such as maximum rebound displacements, contact time and so on. If such expressions could be determined, they would be

evaluated and a check made to ensure that the parameters were within the range required to make solution A valid. The process would be repeated for all of the possible forms of the solution, perhaps resulting in more than one valid displacement expression.

Unfortunately, the Poynting-Thomson model adds an additional unknown, K_2 , to those necessary for the Kelvin-Voigt solution. An additional equation involving the coordinate X_2 is also provided, but as X_2 has no physical meaning, it gives little insight into the problem. No additional relationships exist between measurable parameters from which closed form expressions for the additional unknown may be derived. It would therefore be necessary to curve fit the parameters to this model, perhaps on a digital computer. Curve fitting is an indirect process which is not particularly well suited to many design situations. For this reason the Poynting-Thomson model was not pursued further in this thesis.

CHAPTER III

EXPERIMENTAL APPARATUS AND PROCEDURE

Apparatus

Mechanical Test Device

The experimental device, Figure 8, consisted of the ballistic suspension of two identical one-inch diameter plane ended round steel bars 10.100 inches long. The support wires (0.010-inch diameter steel) were spaced in machined guide blocks which located them within 0.010 inch. Each wire was provided a length adjusting screw (A). The guide blocks could be adjusted into the same level plane (B) and made parallel (C). The wires were attached to the bars by symmetrical aluminum rings.

Initial displacements were made and simultaneous release of the penduli obtained by use of two electromagnets mounted on a track below the penduli and fixed in place with set screws. The magnets were designed so that the field was negligible when the penduli first rebounded. This was done by making the holding force marginal and was verified by experiment.

The pendulus length was such that $\theta \approx \sin \theta$ within 1 per cent for displacements less than five inches.

Instrumentation

Two Valtec photovoltaic cells were used as transducers for the displacement histories of the penduli during rebound. Biasing circuits, Figure 9, were used to improve the photo cells' linearity. As the two

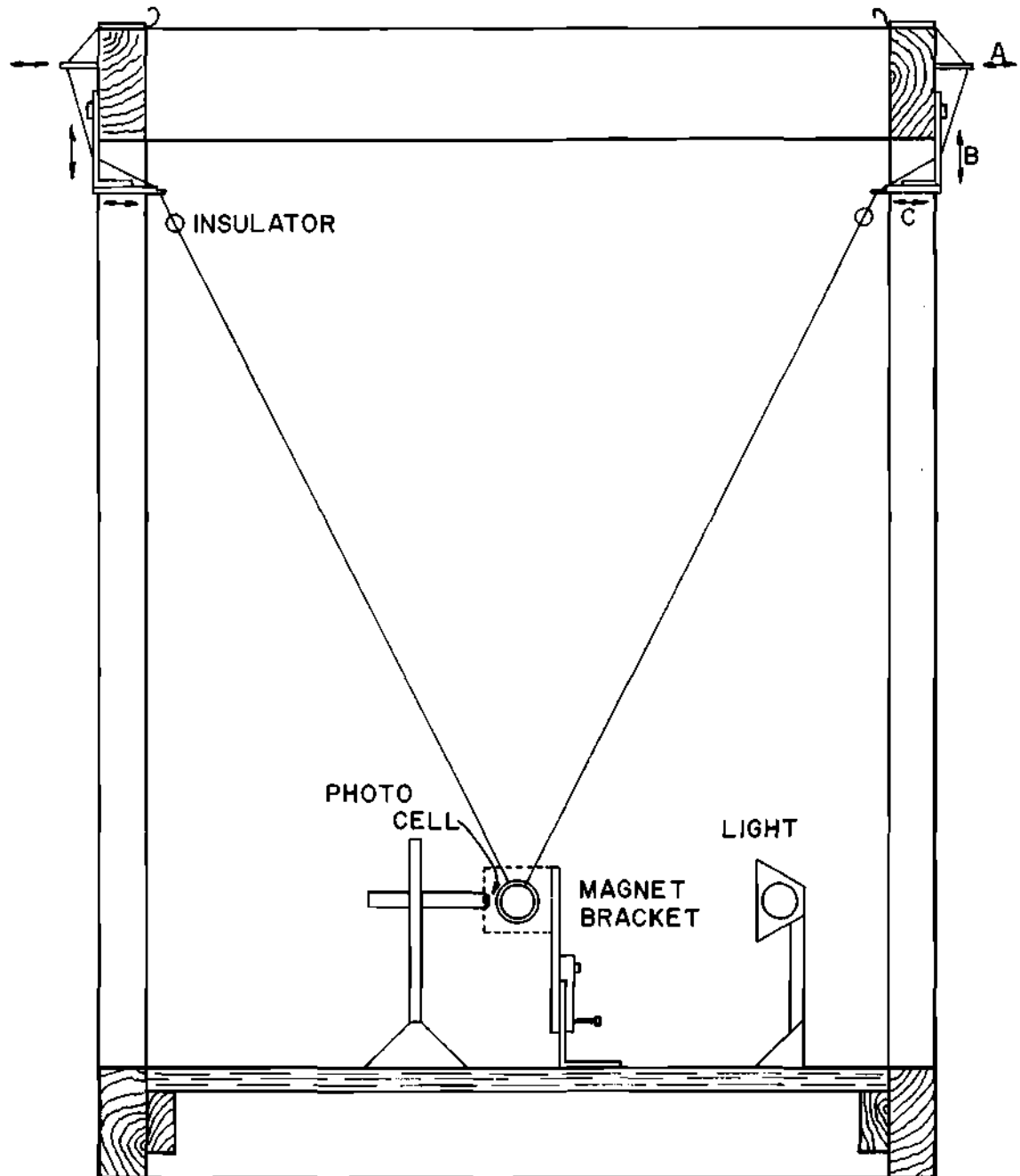


Figure 8. Experimental Test Device

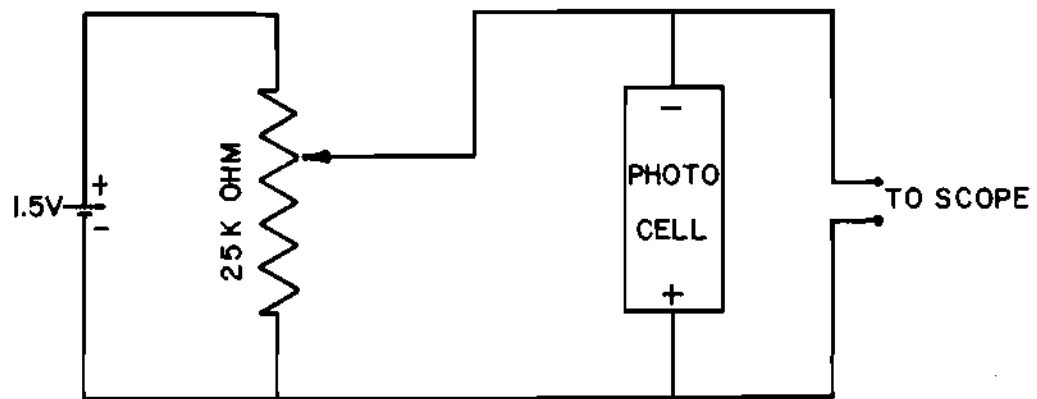


Figure 9. Photocell Biasing Circuit

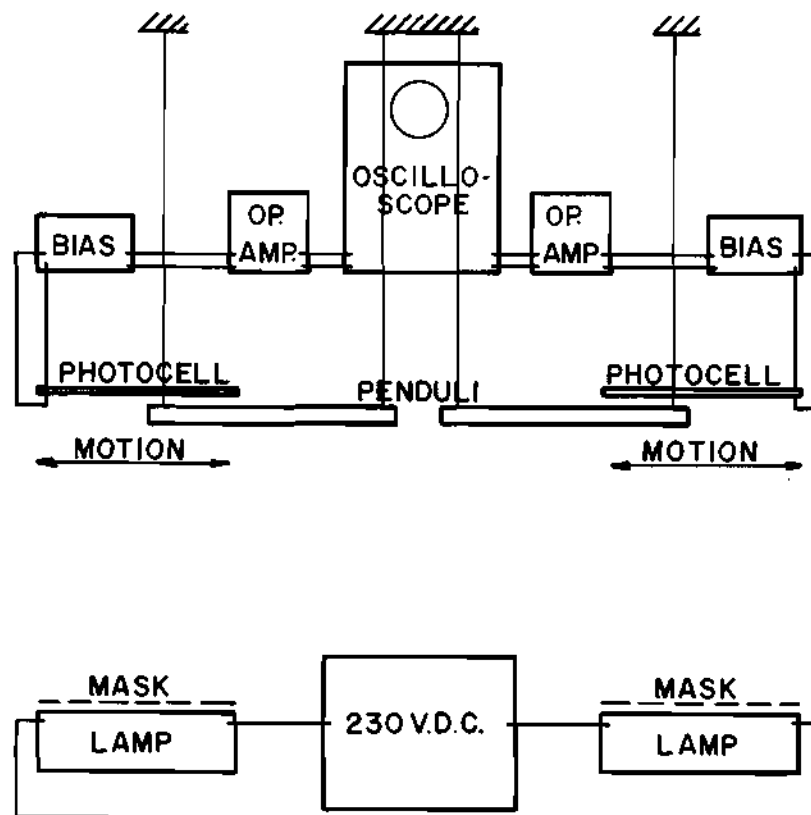


Figure 10. Displacement Transducers

photo cells were not identical, an operational amplifier oscilloscope plug-in was used to partially equalize their gains. Display lamps masked with vellum and powered by a regulated direct current power supply provided illumination to the photo cells. The penduli acted as shutters, admitting illumination to the photo cells inversely proportional to their displacement (Figure 10). The signals from the photo cells were recorded on oscillographs made with a cathod ray oscilloscope and a Polaroid oscilloscope camera.

Contact duration was measured by a circuit which used the penduli as a switch (Figure 11). The signal from this circuit was also recorded on the oscillograph.

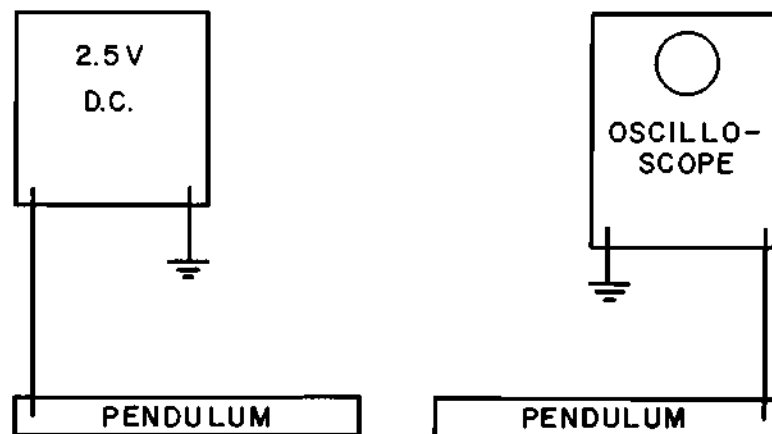


Figure 11. Contact Time Instrumentation

Triggering of the oscilloscope sweep was accomplished by the magnet release circuit, Figure 12. A dual trace oscilloscope plug-in was used to record the displacement signals, leaving the second beam of the oscilloscope for the contact time trace which was triggered by an

internal sweep delay circuit. Two time bases were used to provide different sweep rates to the displacement and contact time traces.

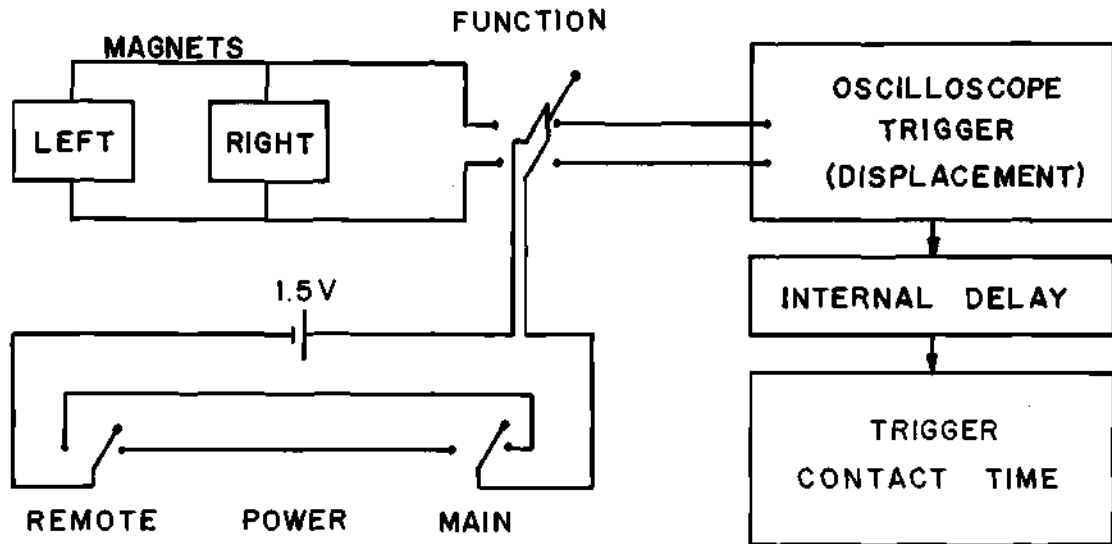


Figure 12. Magnet Release Circuit

Table 1 lists all of the major components used in the experimentation.

Table 1. Experimental Equipment

Dual Beam Oscilloscope	Tektronics Type 555
Oscilloscope Time Base	Tektronics Type 21A
Oscilloscope Time Base	Tektronics Type 22A
Operational Amplifier Plug-In	Tektronics Type 0
Dual Trace Plug-In	Tektronics Type CA
Oscilloscope Camera	Tektronics Series 125
Camera Film Back	Polaroid Series 100

Table 1. Experimental Equipment (Continued)

Regulated D.C. Power Supply	Hewlett Packard Model 721A
Regulated D.C. Power Supply	Kepco Model 430D
Photovoltaic Cell	Valtec Number 7-S50LB
Photovoltaic Cell	Valtec Number 7-S150LB
4" 25w-125v Incandescent Display Lamp (2)	Sears Roebuck and Company
Weatherproof Lamp Socket (2)	Sears Roebuck and Company
Aluminum Lamp Reflector & Mask (2)	Fabricated for the Experiment
NEDA #900 1-1/2 volt Dry Cell (3)	Eveready Number 735
Potentiometer 25k 5% (2)	Centralab Number KS14381-L19
Potentiometer 1meg 5% (2)	Centralab Number RV4NAY-SD105B
SPDT Switch (2)	Cuttler-Hammer Number AN3022-15B
DPDT Switch	Cuttler-Hammer 15A-125V
Micarta Insulator (24)	0.25"x0.25"x0.032"
Assorted Electrical Wire	Cut to Length
Electromagnet (2)	Fabricated for Experiment (Appendix B)
Magnet Holder (2)	Fabricated for Experiment (Appendix C)
Magnet Holder Track	Fabricated for Experiment 3"x2"x3/16" Al. Angle
Support Wire Guide (2)	Fabricated for Experiment (Appendix C)
Wire Guide Support Bracket (2)	Fabricated for Experiment (Appendix C)

Table 1. Experimental Equipment (Continued)

Test Bar Support Ring (4)	Fabricated for Experiment (Appendix C)
0.010" Steel Wire	Driver-Harris Company
Steel Mass (2)	Fabricated for Experiment (Appendix C)
Assorted Structural Elements	Automat Corporation
Wooden Frame	Fabricated for Experiment (Appendix C)
Cathotometer	Gaertner Scientific Company
Vernier Calipers	Lufkin Number 701ME
Framing Square	Craftsman Number 39641
7X Magnifier	Peak Inc.
Milling Machine Bed	Milwaukee Model H

Experimental Procedure

Set Up and Calibration

The guide blocks for the support wires were adjusted into the same level plane using the vertical adjusting screws and a cathotometer. A framing square was used to ensure that the guide blocks were parallel and to locate the support wire slots directly opposite each other. Two plumb lines were dropped from cross bars to locate the magnet support track. Machined center lines in the aluminum support rings served to optically align the radial position of the rings on the bars while simultaneously the axial locations of the rings were set with vernier

calipers. The cathotometer was used to locate the bars parallel to the level guide blocks and equidistant between them. Each support wire was adjusted until the bars were level, co-axial and touching at rest with virtually no normal force between them. Prior to installation in the device, the bars had been wet ground to precisely the same length providing flat impact surfaces and identical masses.

After the installation was complete, the pendulum length L was measured with the cathotometer, which is equipped with an optical level mounted on a vertical vernier scale. With one mass tied back, the other was permitted to oscillate freely and its period was measured on the oscilloscope. This was done to verify that the structural damping was negligible as assumed and to be certain that residual magnetic fields which might be present after the magnet circuits were opened were small enough that their effect might be neglected. The process was then repeated for the other mass.

Initial displacements were established in the following manner. First the cathotometer was used to extend the line defined by the touching end planes of the test bars to the magnet support track. This line, the line of static equilibrium (P.O.E.), was marked by a strip of tape. The magnet supports were then placed equidistant from this line. The initial displacements having been thus roughly established, one magnet support was locked in place. The other magnet support was adjusted by trial and error until the oscilloscope displacement trace displayed minimum oscillation of the line of impact about the line of static equilibrium. The second magnet support was then locked in place.

Finally the bars were pulled against the magnets and the resulting gap was measured with a vernier caliper. The initial displacement of each bar from the position of static equilibrium was taken to be half this measured distance.

After some initial experiments to determine the bias voltage yielding the most linear output from each photocell, the cells were calibrated in the following manner. One mass was retained clear of the other. The second mass was pulled up against the inactive magnet and released. This trace was photographed and replotted on graph paper along with the displacement-time curve of a freely oscillating pendulum of mass M and pendulum length L , calculated by the digital computer program CALIBR, Appendix D (see Figure 13).

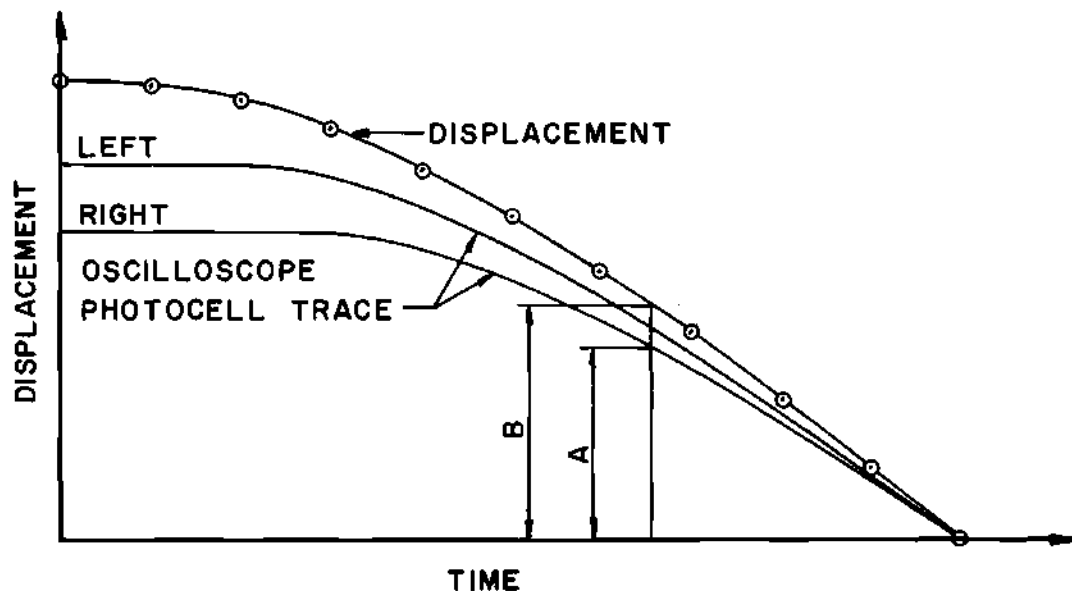


Figure 13. Plot of Oscilloscope Trace and Pendulum Displacement

A calibration curve for the cell, Figure 14, was determined by comparing the output of the cell to the pendulum displacement at several different times.

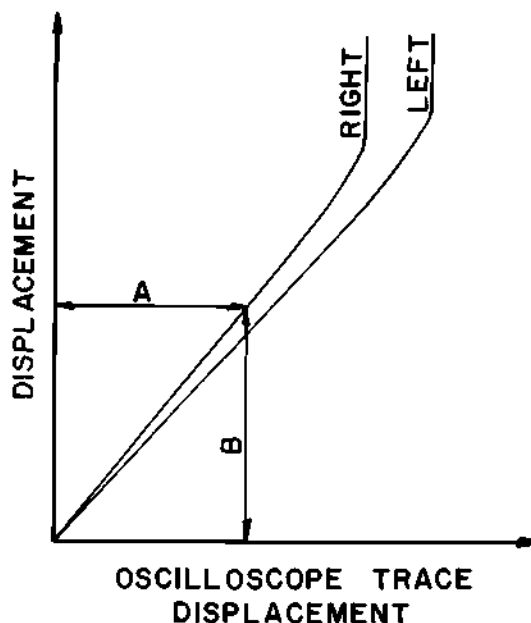


Figure 14. Photocell Calibration Curve

This process was repeated for the other cell and these curves used to evaluate data taken at this set of initial conditions. New calibration curves were established in this manner with each set of new initial displacements. This calibration technique provided dynamic calibration curves and permitted direct reading from the oscilloscope photographs which were in no convenient scale.

By trial and error the internal sweep delay in the oscilloscope was set to display the output signal of the contact time circuit during

the second impact. This trace was essentially a unit step initiated at contact and broken when contact was lost.

Typical Run Procedure

For each set of data the following procedure was followed.

1. Check specimen alignment and ensure that the initial displacements are symmetric to the line of static equilibrium.
2. Measure the initial displacements and pendulum length L .
3. Photograph the photocell calibration curves as described previously.
4. Set the oscilloscope internal sweep delay to record the contact time trace for the second impact.
5. Pull the penduli against the electromagnets, open the oscilloscope camera shutter and release the penduli by putting the function switch in the trigger position. This also triggers the oscilloscope trace, Figure 12.

The required test data is recorded on a single oscillograph in three traces, right and left penduli displacement histories and the contact time trace for the second impact. From this oscillograph the period of contact of the second impact and any maximum rebound displacement may be read. As indicated on page 20, these are sufficient data to determine the Kelvin-Voigt parameters K and C . The displacement histories on the oscillograph may also be compared with the theoretical displacement given by equation 30.

Reduction of Data

The experimental data was reduced from the oscillographs as follows. First the rebounds were numbered as indicated in Figure 15.

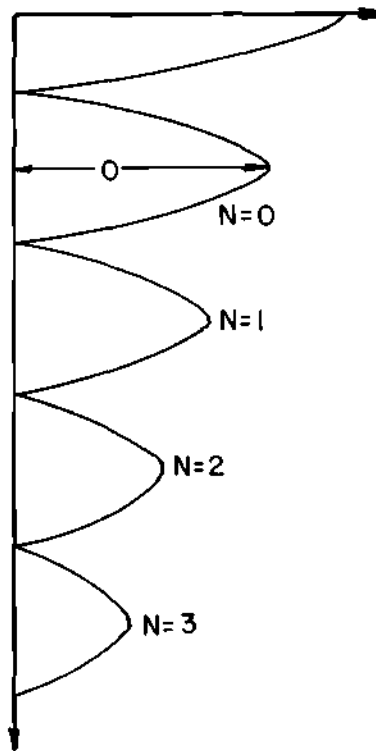


Figure 15. Enumeration of Rebounds from Oscillograph

This method of enumeration accomplished two objectives; it eliminated the need to work with the highly non-linear portion of the photo cell output which occurred when the specimens were very near the magnets and it further ensured that the magnetic fields had completely dissipated and were not affecting the remainder of the response. With this enumeration adopted, the "initial displacements" became the rebound indicated

as "0" in the figure. Since it was not possible to eliminate all oscillation of the point of impact about the position of static equilibrium, displacements were determined by measuring the displacement trace of the right pendulum on the oscillograph and converting it to real displacement using the appropriate calibration curve, repeating the process for the left pendulum and averaging the two real displacements. It is this average displacement which is plotted in the data-theory correlation section of the thesis. The measurements were made by taping the oscillograph to a flat plate clamped to a milling machine table and indexing the photograph relative to an indicator suspended from the milling head. A seven power magnifier was used to aid in locating the indicator on the oscillograph. The ordinate and abscissa were then read from the cross-feed verniers of the milling table. This same process was used to measure the contact time trace and to read the photo cell calibration curves.

CHAPTER IV

CORRELATION OF THEORETICAL AND EXPERIMENTAL RESULTS

Generation of the Theoretical Response Curves

In order to facilitate computation of the theoretical Kelvin-Voigt pendulus impact response curves, a program was written in the FORTRAN algorithmic language for the Univac 1108 digital computer. The program PENDUL, Appendix E, has the capability of reading parameters M , L , X_0 , X_{1m} , and τ_c (pendulum mass, pendulum length, initial displacement, maximum displacement for the first rebound and contact duration) and from them calculating the values of K , C , τ_r (Kelvin-Voigt spring constant and viscous damping coefficient, rebound duration) and the theoretical response for any number of rebounds at any time increment desired. An alternate option in the program allows the theoretical response to be calculated when M , L , X_0 , K and C are specified. Under this option rebound and contact durations (τ_r, τ_c) are also predicted. A third option permits the use of experimental data to calculate the Kelvin-Voigt parameters as in the first option and then predicts the theoretical responses for any number of new initial conditions using the values of the Kelvin-Voigt parameters calculated previously.

Comparison of Theoretical and Experimental Response

The computer program PENDUL was used to calculate the theoretical response for four rebounds for each set of experimental data obtained.

Table 2 lists the error in the maximum rebound displacements for each set of data. The rebounds used to calculate the theoretical data for each initial displacement are easily recognized from Table 2 as those rebounds having zero deviation of the theoretical from the experimental results and are marked by an asterisk.

Table 2. Deviation of Theoretical Response
from Experimental Response

Initial Displace- ment	Rebound Number	Experi- mental X_{\max}	Theoretical X_{\max}	Devia- tion Inches	Deviation % of Peak	Deviation % of X_0
0.115	0*	0.068	0.068	0.000	00.0	00.0
0.115	1*	0.052	0.052	0.000	00.0	00.0
0.115	2	0.029	0.039	+0.010	34.5	08.7
0.115	3	0.029	0.030	+0.001	03.4	00.9
0.115	4	0.016	0.023	+0.007	43.8	06.1
0.234	0*	0.176	0.176	0.000	00.0	00.0
0.234	1*	0.117	0.117	0.000	00.0	00.0
0.234	2	0.091	0.078	-0.013	14.3	05.6
0.234	3	0.060	0.052	-0.008	13.3	03.4
0.234	4	0.034	0.035	+0.001	2.9	00.4
0.323	0	0.225	0.259	+0.034	15.1	10.5
0.323	1*	0.169	0.169	0.000	00.0	00.0
0.323	2*	0.110	0.110	0.000	00.0	00.0
0.323	3	0.073	0.072	-0.001	01.4	00.3
0.323	4	0.062	0.047	-0.015	24.2	04.6
0.405	0*	0.293	0.293	0.000	00.0	00.0
0.405	1*	0.195	0.195	0.000	00.0	00.0
0.405	2	0.117	0.129	+0.012	10.3	03.0
0.405	3	0.060	0.085	+0.025	41.7	06.2
0.405	4	0.053	0.057	+0.004	07.0	01.0
0.478	0*	0.345	0.345	0.000	00.0	00.0
0.478	1*	0.273	0.273	0.000	00.0	00.0
0.478	2	0.206	0.215	+0.009	04.3	01.9
0.478	3	0.141	0.170	+0.029	20.6	06.1
0.478	4	0.107	0.134	+0.027	25.2	05.6

Table 2. Deviation of Theoretical Response
from Experimental Response (Continued)

Initial Displace- ment	Rebound Number	Experi- mental X_{\max}	Theoretical X_{\max}	Devia- tion Inches	Deviation % of Peak	Deviation % of X_0
0.598	0*	0.416	0.416	0.000	00.0	00.0
0.598	1*	0.312	0.312	0.000	00.0	00.0
0.598	2	0.234	0.235	+0.001	00.4	00.2
0.598	3	0.168	0.176	+0.008	04.8	01.3
0.598	4	0.146	0.133	-0.013	08.9	02.2
0.713	0*	0.510	0.510	0.000	00.0	00.0
0.713	1*	0.411	0.411	0.000	00.0	00.0
0.713	2	0.302	0.331	+0.029	09.6	04.1
0.713	3	0.172	0.267	+0.095	55.2	13.3
0.713	4	0.175	0.215	+0.040	22.9	05.6
1.519	0	1.0212	0.893	-0.128	12.5	08.4
1.519	1*	0.679	0.679	0.000	00.0	00.0
1.519	2*	0.516	0.516	0.000	00.0	00.0
1.519	3	0.386	0.392	+0.006	01.7	00.3
1.519	4	0.300	0.298	-0.002	00.6	00.1

* This rebound used to determine Kelvin-Voigt parameters.

It should be noted that especially for low initial displacements, deviations from the experimental response, while several per cent of the respective rebound maximum displacements, are only on the order of a few thousandths of an inch.

It was apparent from the experimental data that some phenomenon, which at first appeared to act randomly on the penduli, caused some rebounds to actually equal or exceed their predecessors in maximum displacement. See, for example, initial conditions 0.115 and 0.713 inches in Table 2. This phenomenon was not predicted by the theoretical model

and accounts for much of the deviation of the theoretical from the experimental responses.

Figures 16, 17 and 18 are plots of the theoretical and experimental responses for three successively larger initial displacements. The phenomenon, rather than increasing in severity as initial displacement is increased, only becomes significant in data from a few initial displacements and appears to some degree in all the displacement records. It may also be seen from these figures that the rebound durations are not strictly constant as had been predicted, although all of the rebound durations were within 7.5 per cent of the theoretical value.

It is felt that both of these unexpected results may be attributed to the effect of an additional forcing function created when the support wires deflect as the penduli impact. This explanation is explored further in Appendix F, although the analysis of this effect was not incorporated into the theoretical development.

Comparison of Theoretical Solutions Using Slightly Varied Parameters

A plot of the measured contact duration versus initial displacement, Figure 19, was made. While the general trend indicated by the solid line appeared, the points were scattered enough to cast some doubt on the accuracy of the contact time measurement. Since one might expect the contact duration to be constant for impacting velocities of the same order of magnitude (equal to the time required for the stress wave to reflect from the far end of the bar and return to the contact surface), it was decided to make some comparisons of the data assuming that all

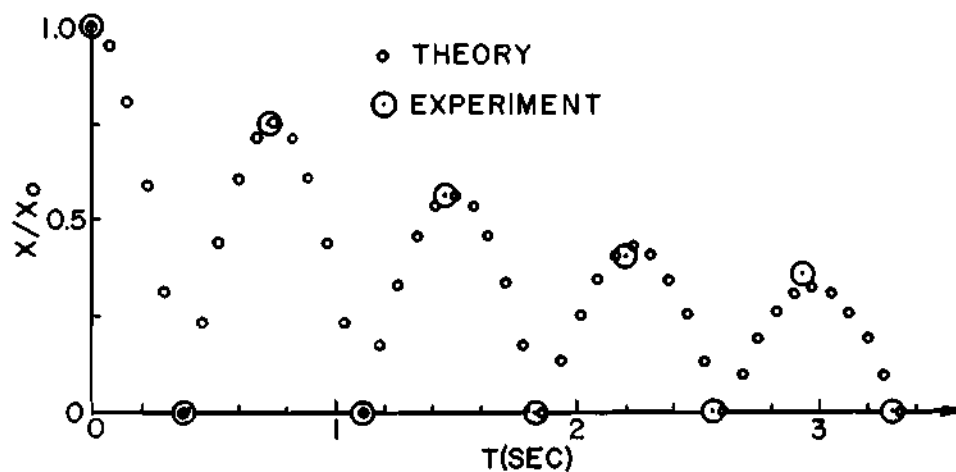


Figure 16. Response for 0.598-Inch Initial Displacement

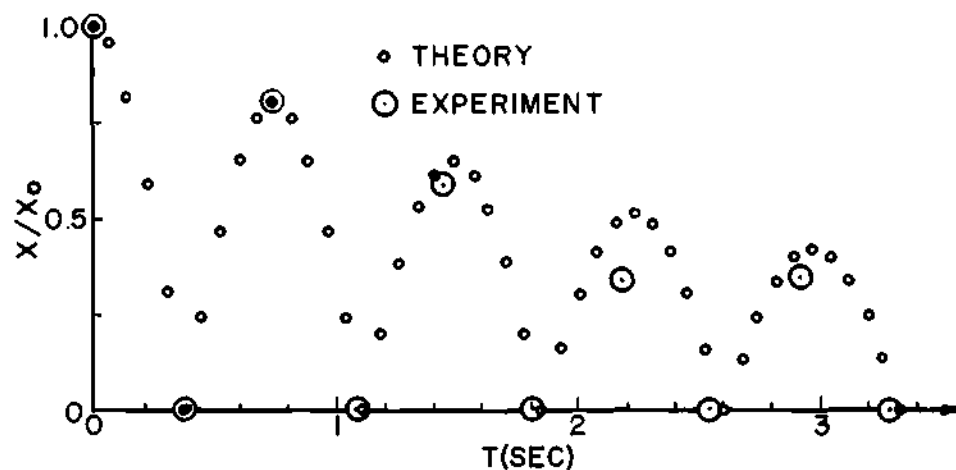


Figure 17. Response for 0.713-Inch Initial Displacement

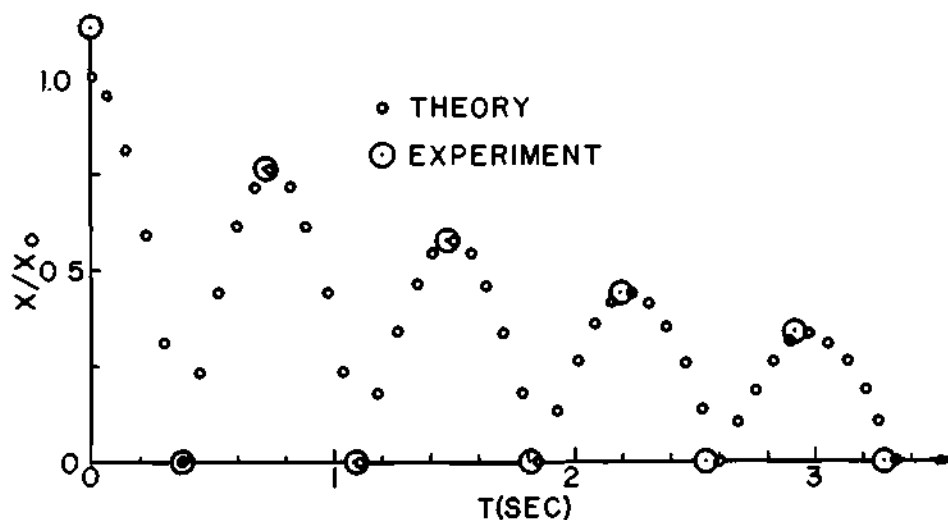


Figure 18. Response for 1.519-Inch Initial Displacement

of the contact durations were of the length of the average contact duration determined experimentally.*

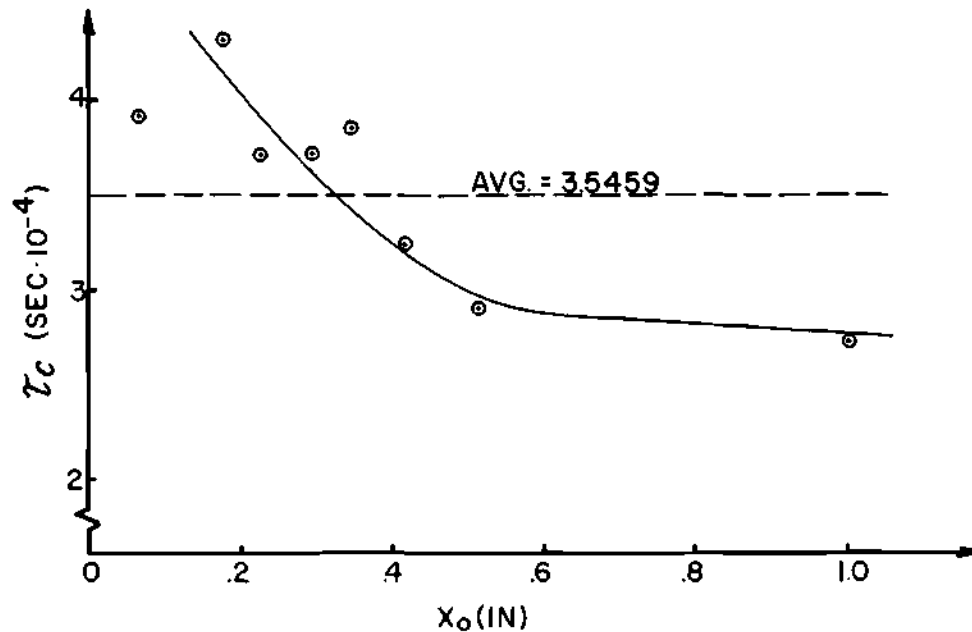


Figure 19. Measured Contact Time Versus Initial Displacement

The theoretical response was computed, using PENDUL, for each of the measured initial displacements and maximum first rebound displacements using the average contact time for all of the data. The peak displacements obtained were identical to the peak displacements which resulted when the individual measured contact times were used. The curves were of course shifted to the left or right proportional to the difference between the individual times and the average contact time.

* By the same order of magnitude it is meant that the velocities are similar enough that no changes in the energy dissipation phenomena occur.

Table 3 lists the values of the Kelvin-Voigt parameter computed using the average experimental contact time versus the square root of the coefficient of restitution for the first rebound and also indicates the per cent deviation in the individual K's compared to the average. It is apparent from the table that the average value of K could be used with an incurred maximum error of only 0.6 per cent.

Table 3. Values of K Versus $\sqrt{\xi}$ for the Bars Tested

$\sqrt{\xi}$	K	ΔK	% Variation
0.8078	465000	3000	0.6
0.8158	464000	2000	0.4
0.8176	464000	2000	0.4
0.8660	460000	2000	0.4
0.8720	460000	2000	0.4
0.8728	460000	2000	0.4
0.8895	460000	2000	0.4
0.8977	459000	3000	0.6
$K_{avg.} = 462000$			

The values of the Kelvin-Voigt viscous damping coefficient C, also computed using the average experimental contact time, were plotted versus the square root of the coefficient of restitution, Figure 20. As seen from the figure, the values described a straight line, the equation for which was determined to be

$$C = 77.44(1 - 1.014\sqrt{\xi}) \quad (40)$$

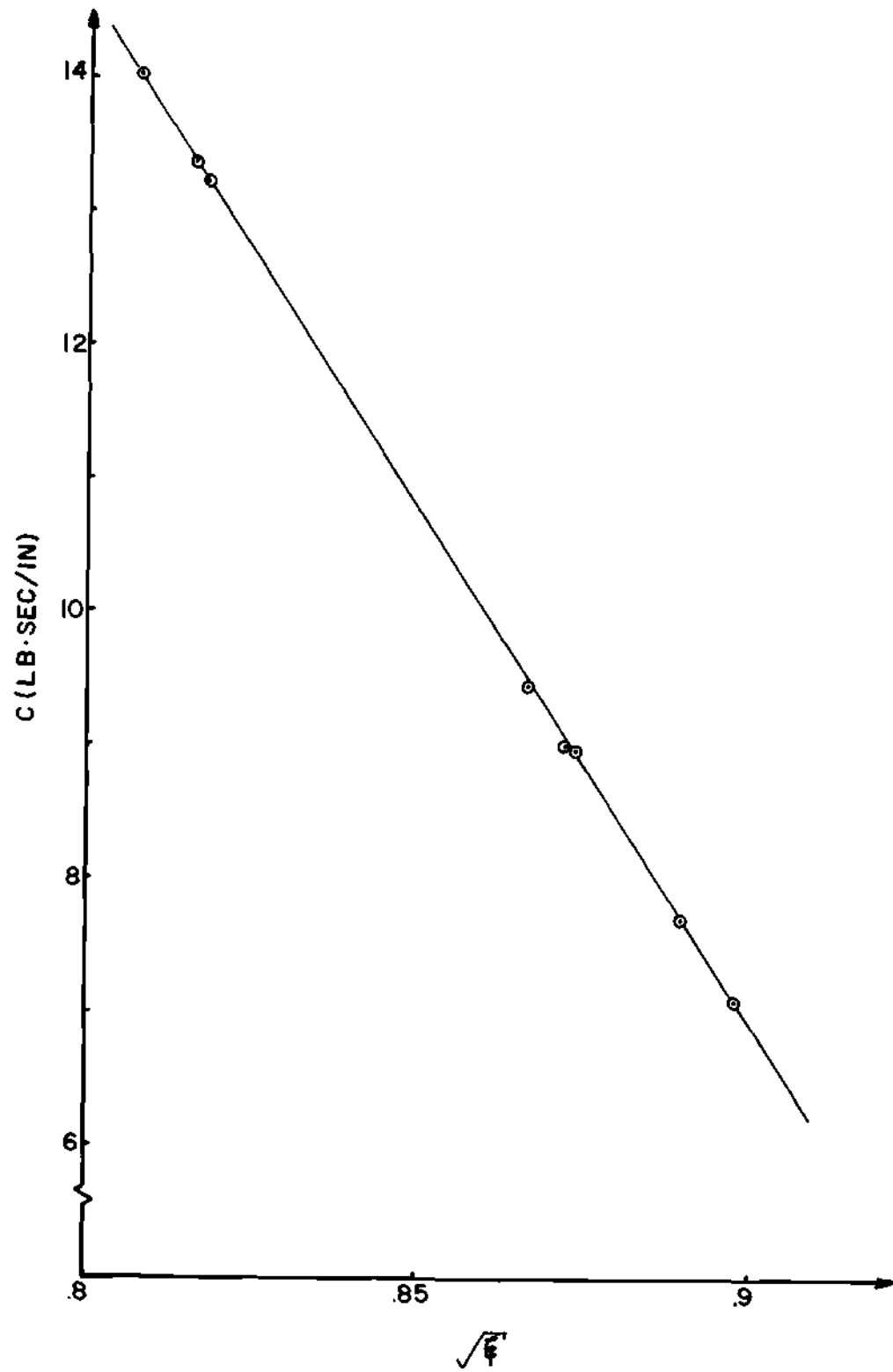


Figure 20. C Versus \sqrt{E} for the Bars Tested

As a final comparison between theoretical responses, the experimental data for the 0.323-inch initial displacement case was used to "predict" the theoretical response for the 0.405-inch initial displacement case using the third option in the PENDUL program. The two particular cases were chosen for this comparison because they displayed nearly the same coefficient of restitution in the experimental data. Table 4 lists both theoretical responses and the deviation of the "predicted" response from the theoretical response based on experimental data.

Table 4. Comparison of Predicted and Calculated Theoretical Response for the 0.405-Inch Initial Displacement Case

Rebound	Predicted X_{\max}	Calculated X_{\max}	Deviation Inches	Deviation % Peak	Deviation % X_0
0	0.293	0.293	0.000	0.0	0.0
1	0.191	0.195	0.004	2.1	1.4
2	0.124	0.129	0.005	3.9	1.7
3	0.081	0.085	0.004	4.7	1.4
4	0.053	0.057	0.004	7.0	1.4

CHAPTER V

CONCLUSIONS AND RECOMMENDATIONS

Rheological Models

The rheological models described in the introduction were created by choosing combinations of mechanical elements whose force deflection equations approximated the force deflection or stress strain curves of the materials for which they were proposed. As the models do not describe the actual energy dissipation phenomena which are present in the collisions of imperfectly elastic bodies, one should not be too surprised that the parameters of the models, which may be chosen to fit the response curves in an individual impact case, are no more independent of impacting velocities (and presumably body geometry) than is the coefficient of restitution; a point of great interest to designers. In fact, it was found that in the cases studied the parameters of the Kelvin-Voigt model could be expressed as functions of the coefficient of restitution. It is the major conclusion of this thesis that the mathematical modeling of imperfectly elastic materials in impact will have to be based on an understanding of the microscopic energy dissipation phenomena involved before much hope can be held for being able to predict responses directly from material properties. This is also the position of G. S. Pisarenko who has been working toward that goal in the Soviet Union.

Some additional conclusions may be drawn regarding the facility of using rheological models as design tools in describing imperfectly elastic impact. Models of complexity equal to or greater than that of the Poynting-Thomson model, while they may allow closer fitting of a displacement equation to experimental data, have limited applicability to the design situation since no closed form expressions for their parameters in terms of easily measured variables may be found. This means that some type of curve fitting routine must be used to fit these models to displacement histories which, perforce, must already exist.

The Kelvin-Voigt model has the advantage that using the closed form expressions of Chapter II and three relatively easy to measure parameters, initial displacement, a maximum rebound displacement and the duration of contact, the system response may be described with some degree of accuracy. This advantage may be exploited further by noting that the contact time is extremely small relative to the period of several rebounds and that errors of several hundred per cent in its value would produce only minute phase shifts in the theoretical response curves. It was demonstrated that changes in the value of this parameter did not affect the predicted rebound maximum displacements at all. In application therefore, the contact time could be estimated, perhaps by considering the perfectly elastic case, reducing to two the number of data required for determining the system parameters. The two remaining values, initial displacement and a maximum rebound displacement, are the easiest of all to obtain experimentally. Simplifying further, for the steel bars of this thesis, it was found that the spring rate K could be fixed

at 462000 pounds per inch and the viscous damping coefficient C determined from equation 40.

It may be concluded that for impacting velocities varying little from one for which the values of K and C are known, those parameter values might be used to predict impact response as demonstrated in the previous section.

It has been pointed out that the Kelvin-Voigt parameters vary with impacting velocity in much the same way as the coefficient of restitution. Unlike the coefficient of restitution which only purports to account for some undescribed form of energy dissipation in impact, rheological models involving viscous damping terms tacitly characterize the form of energy dissipation--hence the term "viscoelastic material." The use of such models then may superficially appear to sophisticate the analysis. Let it be stated here that the Kelvin-Voigt rheological model formulation of equation 30 because it uses the rheological model only as an energy dissipator between rebounds, produces response curves identical to those which would be obtained in pendulus impact if the coefficient of restitution alone were used. This is true because equation 30, rewritten below,

$$x = [(-1)^N (\dot{x}_0 \sqrt{1/g} / \sqrt{1-\xi^2}) e^{-\xi \omega_n N T_c} \cos(N\pi + \phi)] \sin \sqrt{g/L} [t - N T_c - (N - 1/2) T_r] \quad (41)$$

could be written

$$X = A(N) \sin \sqrt{g/L} [t - N\tau_c - (N - 1/2)\tau_r] \quad (42)$$

where

$$A(N) = (-1)^N (\dot{X}_0 \sqrt{L/g} / \sqrt{1 - \xi^2}) \cos(N\pi + \phi) e^{-\xi \omega_n N \tau_c} \quad (43)$$

In equation 43 the minus one to the N term serves only to make the bracketed term positive for all values of N. (And thus for all values of $\cos(N\pi + \phi)$.) Equation 43 could therefore be written

$$A(N) = \dot{X}_0 \bar{A} e^{-\xi \omega_n N \tau_c} = \dot{X}_0 \bar{A} (e^{-\xi \omega_n \tau_c})^N = \dot{X}_0 \bar{A} (E)^N \quad (44)$$

where E is analogous to the coefficient of restitution.

The Experimental Device

The most important difficulty which was experienced with the experimental device was the effect which the support wires had on the impact response (see page 38 and Appendix F). This effect definitely distorted the experimental data and made comparison with the theoretical results difficult. In order to better study the facility of rheological models in describing impact response it would be necessary either to include the support wire effect in the analysis or to isolate it from the experimental apparatus.

Perhaps the best way to avoid the problem experimentally would be to eliminate it entirely, which of course would preclude the use of a pendulum device. Two possible experimental alternatives are offered, each with its own disadvantages.

One approach might be to study solid spheres dropping onto a massive hardened steel plate using a high-speed motion picture camera to record the response, perhaps with a scaled rectangular grid as a back drop. This technique would obviously eliminate the support wire difficulty of the pendulum device but it would also make the present method of contact duration measurement impossible. It must be anticipated that the sphere would not rebound along a strictly vertical line, though this might be of little significance as long as the sphere did not bounce off of the plate or out of the camera's field of view. Finally, this approach would complicate the problem by involving the properties of the target plate in the analysis.

Another alternative device might consist of an arc-shaped or parabolic track of concave cross section which, mounted in the vertical plane, would allow two test spheres to collide and rebound about a position of static equilibrium. Such an approach would again require the use of high-speed photography to record the displacement histories of the spheres but would ensure that the experimental objects remained within the field of view. The elimination of the target plate of the first alternative would be advantageous but the problem of the spheres slipping on the track and the added effect of rolling impact detract from this design. Increased difficulty in the measurement of contact duration is also present in this device.

Measurement of the contact duration was definitely not as accurate as could be desired. As indicated, both of the alternative experimental devices, while they ameliorate some other difficulties, only compound this problem. An improved contact time measurement might be made by an electronic circuit, triggered by much lower voltage than that used in the present apparatus (2.5v) which would provide pulses at the initiation and cessation of contact and which might be connected to a digital clock.

Observation of the impact surfaces after all the experimentation was completed indicated that contact had not been planar but had occurred along one edge of the test bar faces. While this probably did not detract severely from the experimental results, it did violate an assumed experimental condition.

It is recommended that further experimental investigations of this type use an apparatus very similar to the one used in this work. It is felt that extensions of the analysis of Appendix F could be used to account for the support wire effect and that this done, the pendulum device would yield satisfactory results at reasonable cost. It is further recommended that the apparatus incorporate the following modifications. First, a contact duration measuring circuit similar to that described earlier should be employed. Second, it would be very desirable to use two photovoltaic cells of identical gain as the displacement transducers. Third, the test specimens should have large radius, crowned impact faces to ensure definable impact conditions. Finally it would be a great advantage to the experimenter to mount the release magnets on a

set of vernier lead screws so that initial displacements could be set accurately and without resorting to a tedious trial and error procedure.

APPENDIX A

DERIVATION OF POYNTING-THOMSON EQUATIONS

From Chapter II, the Poynting-Thomson model has the following equations of motion.

$$\begin{aligned}\ddot{X}_1 + (K_1 + K_2)X_1/M - K_2X_2/M &= 0 \\ C\dot{X}_2 - K_2X_1 + K_2X_2 &= 0\end{aligned}\tag{45}$$

Initial conditions are $X_1(0) = X_2(0) = \dot{X}_2(0) = 0$ and $\dot{X}_1(0) = \dot{X}_{10}$.

The Laplace transformations of equations 45 are (6)

$$\begin{aligned}(s^2 + D)\hat{X}_1 - E\hat{X}_2 &= \dot{X}_{10} \\ -K_2\hat{X}_1 + (Cs + K_2)\hat{X}_2 &= 0\end{aligned}\tag{46}$$

where

$$D = (K_1 + K_2)/M, \quad E = K_2/M.\tag{47}$$

By Cramer's Rule,

$$\hat{X}_1 = \frac{\begin{vmatrix} \dot{X}_{10} & -E \\ 0 & (Cs + K_2) \end{vmatrix}}{\begin{vmatrix} (s^2 + D) & -E \\ -K_2 & (Cs + K_2) \end{vmatrix}} = \frac{(s + K_2/C)\dot{X}_{10}}{s^3 + s^2 K_2/C + sD + K_2(D-E)/C} \quad (48)$$

$$\hat{X}_2 = \frac{\begin{vmatrix} (s^2 + D) & \dot{X}_{10} \\ -K_2 & 0 \end{vmatrix}}{\begin{vmatrix} (s^2 + D) & -E \\ -K_2 & (Cs + K_2) \end{vmatrix}} = \frac{\dot{X}_{10} K_2/C}{s^3 + s^2 K_2/C + sD + K_2(D-E)/C} \quad (49)$$

In order to find the inverse transforms, the denominator (characteristic equation) must be factored. A term $(s+p)$ is a factor if it can be divided evenly into the denominator; that is with a null remainder. Division of the denominator by $(s+p)$ yields a quadratic with remainder

$$(p^3 - p^2 K_2/C + pD - K_1 K_2/CM)/(s+p) = 0 \quad (50)$$

The term $(s+p)$ is a factor of the characteristic equation for all p 's which are roots of equation 50.

According to the scheme of reference 7, let

$$a = D - K_2^2/3C^2$$

$$b = (9K_2D/C - 2K_2^3/C^3 - 27K_1K_2/CM)/27$$

$$d = \sqrt{b^2/4 + a^3/27} \quad (51)$$

$$A = \sqrt[3]{d - b/2}$$

$$B = \sqrt[3]{-d - b/2}$$

Then

$$P_1 = A + B + K_2/3C$$

$$P_2 = K_2/3C - (A + B)/2 + [(A - B)\sqrt{3}/4]i \quad (52)$$

$$P_3 = K_2/3C - (A + B)/2 - [(A - B)\sqrt{3}/4]i$$

Note that if $d > 0$ there will be one real root and two complex conjugates and if $d = 0$ there will be three real roots, at least two of which are equal. If $d < 0$ there will be three real and unequal roots.

For case I, $d > 0$, equation 48 may be written

$$\hat{X}_1 = \frac{(s + K_2/C) \dot{X}_{10}}{(s + p_1)[(s + P)^2 + \omega^2]} \quad (53)$$

where

$$\begin{aligned} P &= K_2/3C - (A + B)/2 & p_2 &= P + \omega i \\ \omega &= (A - B) \sqrt{3}/4 & p_3 &= P - \omega i \end{aligned} \quad (54)$$

The inverse transform of equation 53 is

$$X_1(t) = \dot{X}_{10} \left[\frac{(-P_1 + K_2/C)}{(P_1 - P)^2 + \omega^2} e^{-P_1 t} + (1/\omega) \sqrt{\frac{(-P + K_2/C)^2 + \omega^2}{(P_1 - P)^2 + \omega^2}} e^{-P t} \sin(\omega t + \phi) \right] \quad (55)$$

where

$$\phi = \arctan[\omega/(-P + K_2/C)] - \arctan[\omega/(P_1 - P)] \quad (56)$$

Equation 49 becomes

$$\hat{X}_2 = \frac{\dot{X}_{10} K_2/C}{(s + p_1)[(s + P)^2 + \omega^2]} \quad (57)$$

and its inverse transform is

$$x_2(t) = \frac{\dot{x}_{10} K_2 / C}{(P_1 - P)^2 + \omega^2} \left[e^{-Pt} + (1/\omega) \sqrt{(P_1 - P)^2 + \omega^2} e^{-Pt} \sin(\omega t - \phi) \right] \quad (58)$$

where

$$\phi = \arctan[\omega / (P_1 - P)] \quad (59)$$

For case II, $d=0$, two subcases may exist. For case IIa, $P_1 = P_2 = P_3 = \frac{K_2}{3C}$, equation 48 may be written

$$\hat{x}_1 = \frac{\dot{x}_{10}(s + K_2/C)}{(s + K_2/3C)^3} \quad (60)$$

Equation 60 has the inverse transform

$$x_1(t) = \dot{x}_{10} (t + t^2 K_2 / 3C) e^{-t K_2 / 3C} \quad (61)$$

Equation 49 becomes

$$\hat{x}_2 = \dot{x}_{10} K_2 / C (s + P)^3 \quad (62)$$

which has the inverse transform

$$X_2(t) = (t^2 \dot{X}_{10} K_2 / 2C) e^{-tK_2/3C} \quad (63)$$

For case IIb, $P_1 = P_1$, $P_2 = P_3 = P$, equation 48 is

$$\hat{X}_1 = \dot{X}_{10} (s + K_2/C) / [(s + P_1)(s + P)^2] \quad (64)$$

and the inverse transform is

$$X_1(t) = \dot{X}_{10} \left\{ \frac{(-P_1 + K_2/C)}{(P_1 - P)} e^{-P_1 t} + \left[\frac{(-P + K_2/C)}{(P_1 - P)} + \frac{(P_1 - K_2/C)}{(P_1 - P)^2} \right] e^{-Pt} \right\} \quad (65)$$

Equation 49 becomes

$$\hat{X}_2 = \dot{X}_{10} K_2 / C (s + P_1)(s + P)^2 \quad (66)$$

which has the inverse transform

$$X_2(t) = \frac{\dot{X}_{10} K_2 / C}{(P_1 - P)^2} \left\{ e^{-P_1 t} + \left[(P_1 - P)t - 1 \right] e^{-Pt} \right\} \quad (67)$$

In case III, $d < 0$, equation 48 becomes

$$\hat{X}_1 = \frac{\dot{X}_{10}(s + K_2/C)}{(s + P_1)(s + P_2)(s + P_3)} \quad (68)$$

Equation 68 has the inverse transform

$$X_1(t) = \dot{X}_{10} \left[\frac{(-P_1 + K_2/C)}{(P_2 - P_1)(P_3 - P_1)} e^{-P_1 t} + \frac{(-P_2 + K_2/C)}{(P_1 - P_2)(P_3 - P_2)} e^{-P_2 t} + \frac{(-P_3 + K_2/C)}{(P_1 - P_3)(P_2 - P_3)} e^{-P_3 t} \right] \quad (69)$$

Similarly, equation 49 becomes

$$\hat{X}_2 = \frac{\dot{X}_{10} K_2/C}{(s + P_1)(s + P_2)(s + P_3)} \quad (70)$$

which has the inverse transform

$$X_2(t) = (\dot{X}_{10} K_2/C) \left[\frac{e^{-P_1 t}}{(P_2 - P_1)(P_3 - P_1)} + \frac{e^{-P_2 t}}{(P_1 - P_2)(P_3 - P_2)} + \frac{e^{-P_3 t}}{(P_1 - P_3)(P_2 - P_3)} \right] \quad (71)$$

In Chapter II all of the coefficients above are represented by subscripted γ 's and all the exponents by subscripted ρ 's.

APPENDIX B

DESIGN OF ELECTROMAGNETS

The electromagnets were designed to retain the penduli at maximum displacements of three inches. For a pendulus length of 22 inches, the force necessary to retain the mass was found to be 0.307 pounds, based on a pendulus weight of 2.23 pounds. As a factor of safety, the maximum design holding force for the magnets was chosen to be one-half pound.

The magnets designed for this application were of the flat faced armature type utilizing the penduli themselves as the armatures. From reference 8, the magnetic flux density required to produce a force F in a flat faced armature magnet of core radius r is given by

$$B = \sqrt{11.45 F / r^2} \quad (72)$$

For this application $F = 0.5$ pounds and $r = 0.25$ inches (see Figure 21) so that a flux density of 9.56 kilomaxwells per square inch is required.

The required ampere-turns are given by

$$NI = 289/\mu + 200r \quad (73)$$

where μ , the permeability, is 0.00319 kilomaxwells per ampere-turn-inch and in this case g , the air gap, is taken to be 0.02 inches. Substitution of these values and the values of B and r given above into equation 73 indicated that 170 ampere-turns were necessary. Using 30 gauge enameled copper magnet wire (resistance = 0.103 ohms per foot) and a 1.5 volt lantern battery, the soft iron mandrel of Figure 21, wound in a close-packed pattern, yielded the desired restraining force. A calculation of the temperature rise in the coil showed this effect to be negligible.

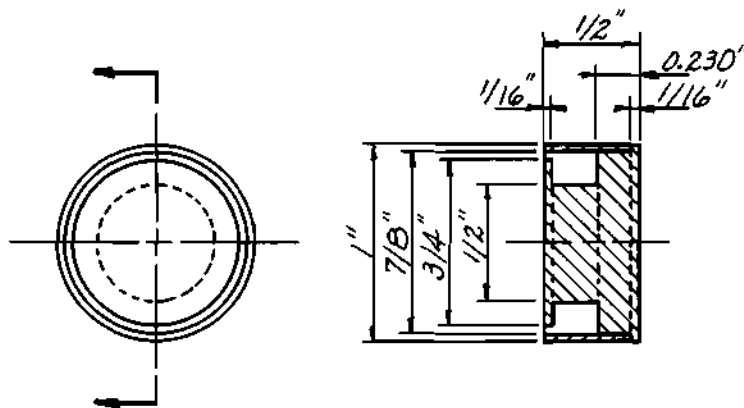


Figure 21. Electromagnet

APPENDIX C

DRAWINGS FOR SELECTED EXPERIMENTAL PARTS

The following figures describe those parts which were fabricated for the experimental work of this thesis and for which duplication would be necessary if it were desired to repeat the condition under which the experiments were conducted. The parts for which drawings have been included in this appendix are:

1. Magnet Holder, Figure 22.
2. Support Wire Guide, Figure 23.
3. Wire Guide Support Bracket, Figure 24.
4. Test Bar Support Ring, Figure 25.
5. Steel Mass, Figure 26.
6. Wooden Frame, Figure 27.

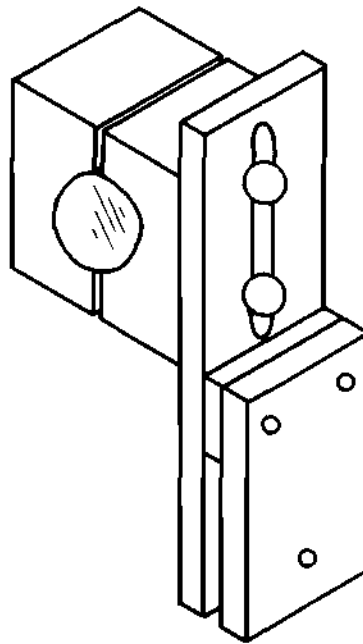


Figure 22. Magnet Holder

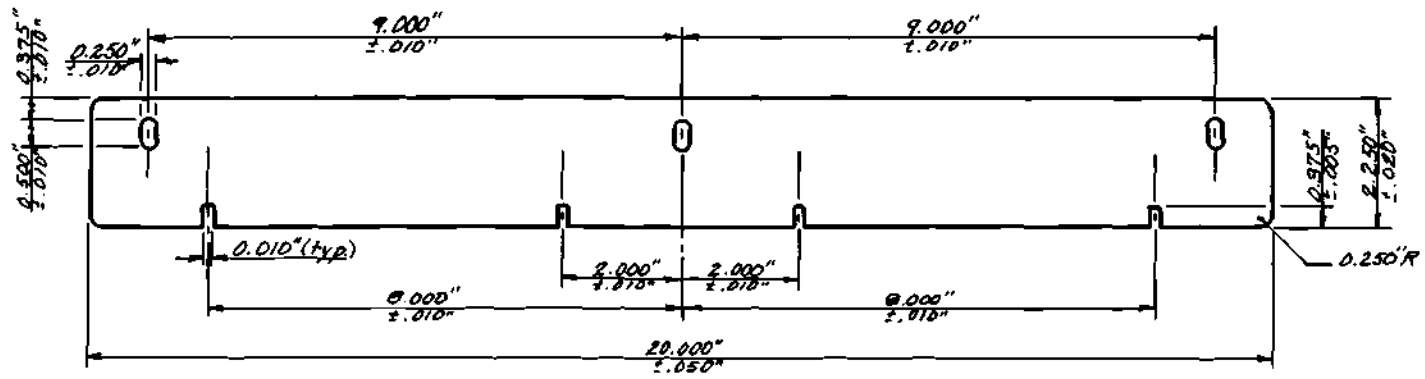


Figure 23. Support Wire Guide

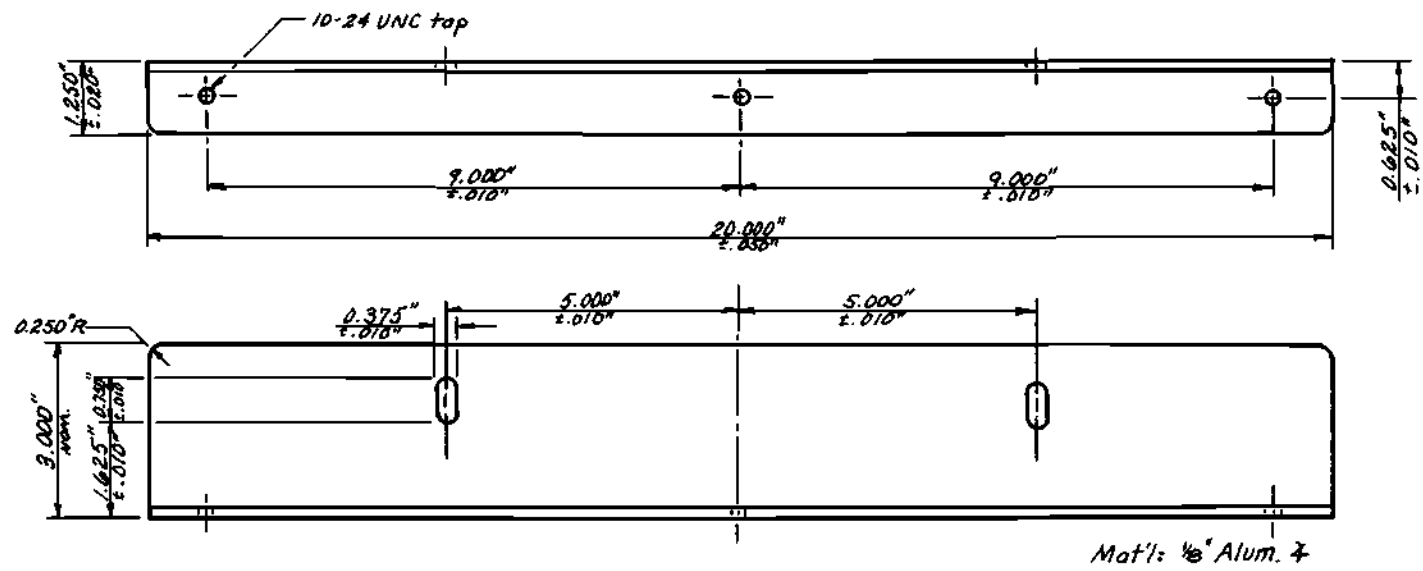


Figure 24. Wire Guide Support Bracket

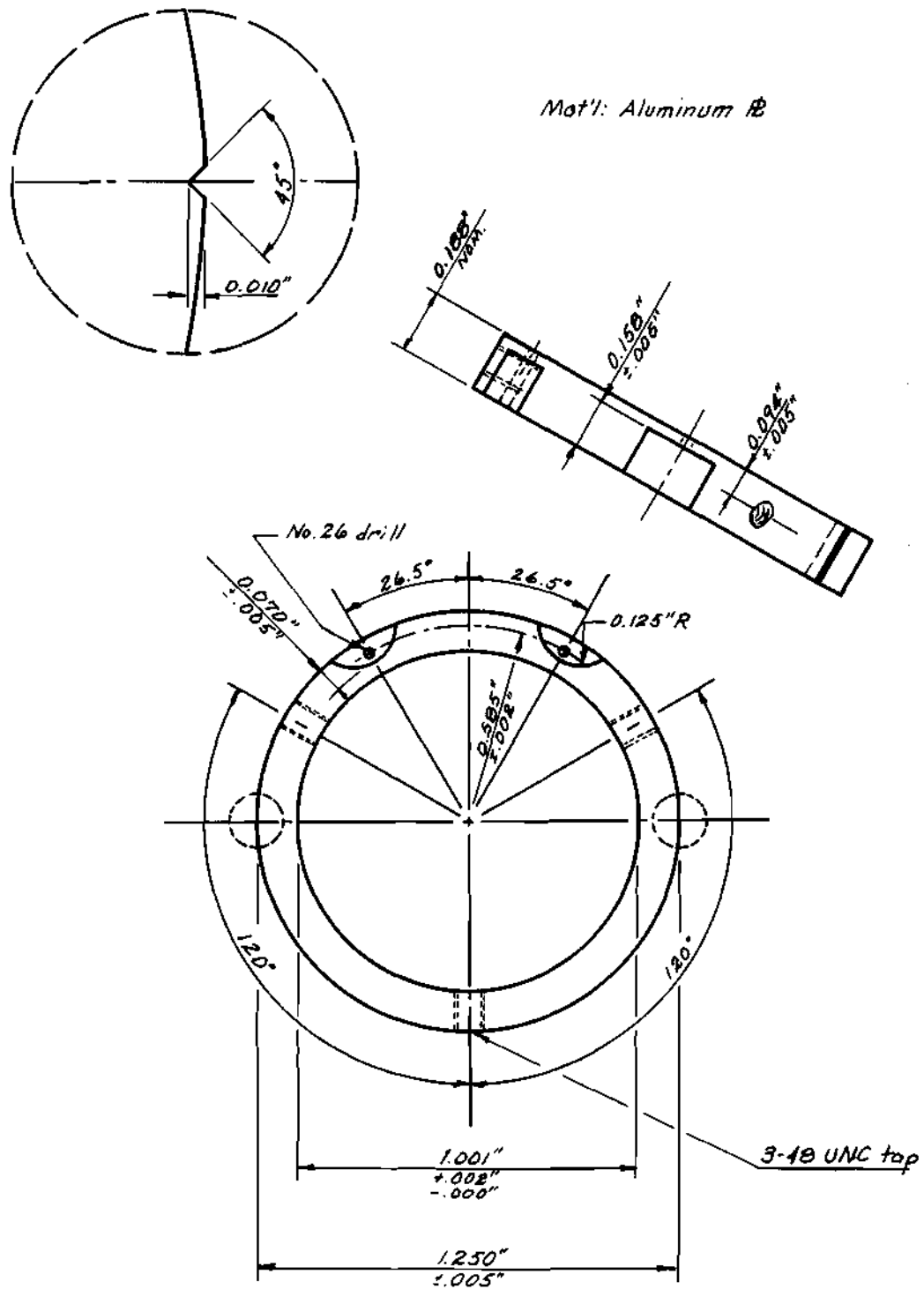


Figure 25. Test Bar Support Ring

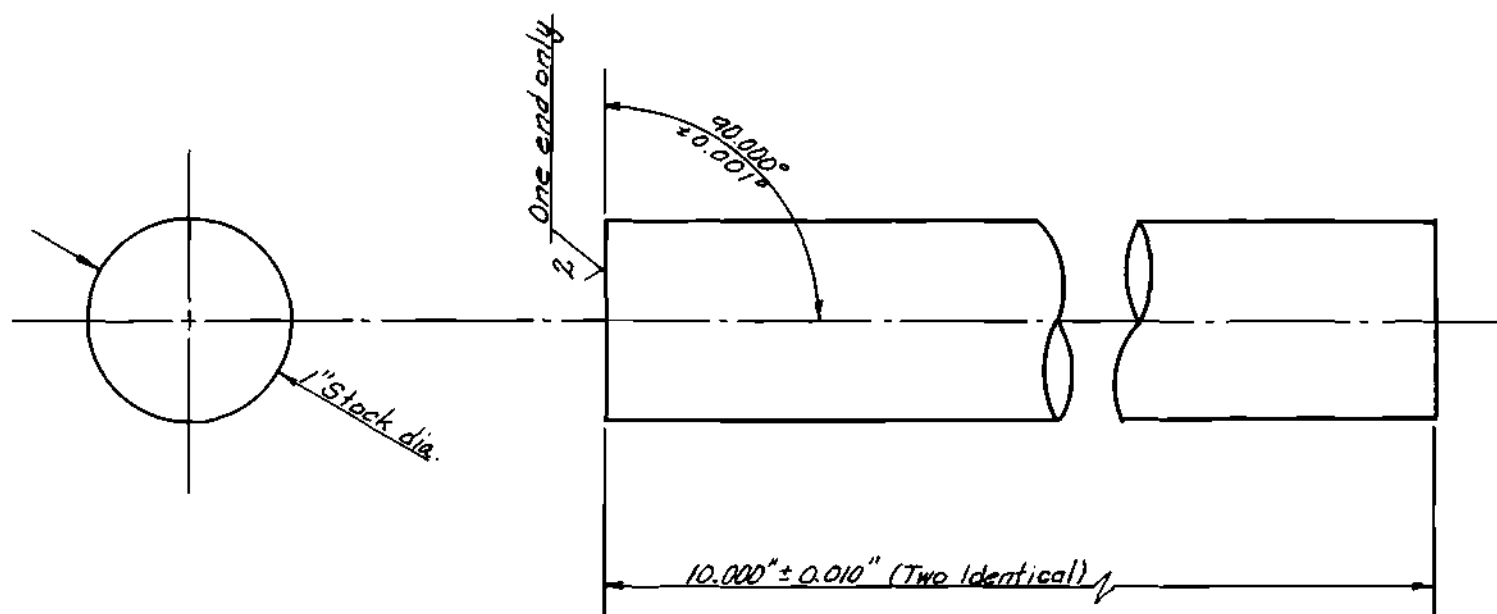


Figure 26. Steel Mass

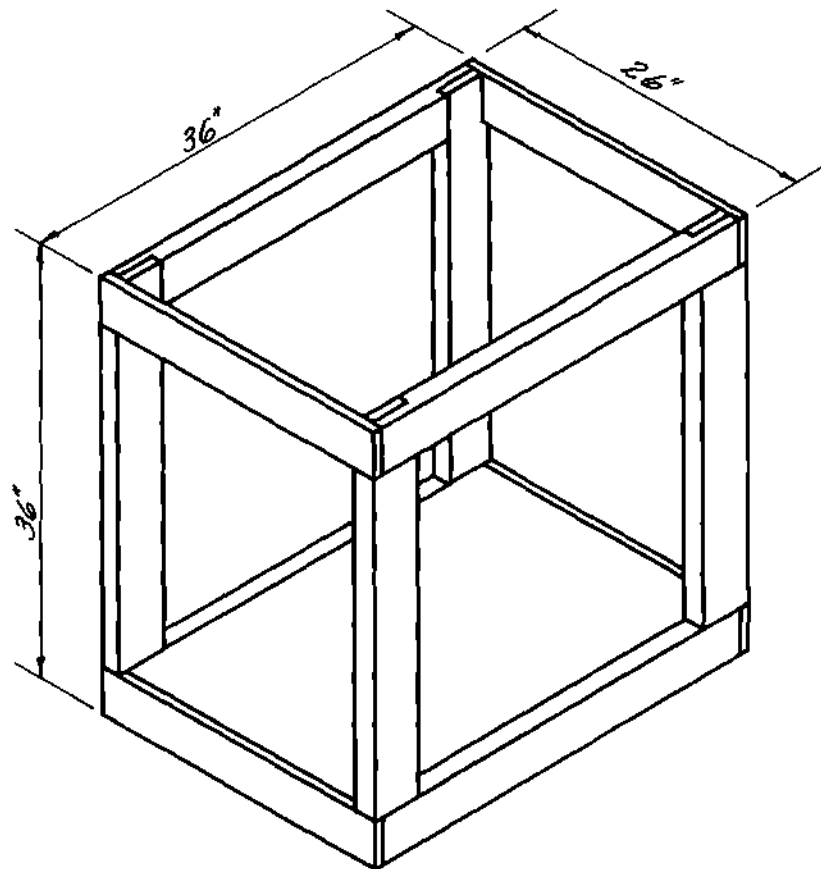


Figure 27. Wooden Frame

APPENDIX D

DIGITAL COMPUTER PROGRAM CALIBR

On the following page a listing of the digital computer program CALIBR is presented. Written in the FORTRAN algorithmic language, CALIBR was used to calculate the displace-time pairs plotted as part of the photo cell calibration procedure of Chapter II.

The input data was as follows: The first data card contained the number of cases to be considered, an integer between one and nine in the first column of the data card. The remaining data cards (maximum of nine) contained the mass of one pendulum, the pendulum length, the initial displacement (all in inch units) for each case to be considered. These data were in free field format, separated by commas.

The program output was in the form of a table of eleven displacement-time pairs for each set of input data, evenly spaced from time zero to the time when the pendulum would cross the line of static equilibrium.

```

1*      DATA G/385.644/,PI/3.14159/
2*      1 FORMAT(I1)
3*      2 FORMAT()
4*      3 FORMAT(/,7X,6HMASS= ,E11.5,8HLENGTH= ,E11.5,4HX0= ,E11.5,//
5*      A,9X,4HTIME,12X,1HX)
6*      4 FORMAT(6X,E11.5,3X,E11.5)
7*      READ(5,1) ICASES
8*      DO 900 I=1, ICASES,1
9*      READ(5,2) BMASS,PL,X0
10*     WRITE(6,3) BMASS,PL,X0
11*     PER=0.5*PI*SQRT(PL/G)
12*     FWN=SQRT(G/PL)
13*     T=0.0
14*     DO 900 J=1,11,1
15*     IF (J.EQ.1) GO TO 800
16*     T=T+0.1*PER
17*     800 X=X0*COS(FWN*T)
18*     IF (ABS(X).LE.1E-5) X=0.0
19*     900 WRITE(6,4) T,X
20*     STOP
21*     END

```

END OF COMPILATION: NO DIAGNOSTICS.

APPENDIX E

DIGITAL COMPUTER PROGRAM PENDUL

The following three pages are a listing of the digital computer program PENDUL. The functions of this program are fully described in Chapter IV. The first few comment statements in the listing give complete input data instructions.

The output of this program consisted of a table of displacement-time pairs for as many rebounds as were desired and at as many equally spaced points in time as necessary. Additionally, the Kelvin-Voigt parameters K and C as well as the pendulum mass, pendulum length, initial displacement, contact time, rebound time and maximum first rebound displacement, whether read in as data or calculated in the program, were displayed.

```

1*   C           *** IMPACTING KELVIN-VOIGT VISCOELASTIC PENDULI ***
2*   C
3*   C   DETERMINATION OF SYSTEM PARAMETERS FOR THE KELVIN-VOIGT VISCO-
4*   C   ELASTIC MODEL AND COMPUTATION OF THEORETICAL DISPLACEMENT FOR
5*   C   INCREMENTAL TIME
6*   C
7*   C
8*   C
9*   C   DATA IS,
10*  C   1. NUMBER OF CASES TO BE RUN, ICASES, NUMBER OF REBOUNDS TO BE
11*  C       CALCULATED, IBOUND, NUMBER OF DATA POINTS DESIRED PER REBOUND,
12*  C       IPOINT, ACCORDING TO FORMAT 1 (IPOINT SHOULD BE AN ODD NUMBER)
13*  C   2. OPTION, OPT, ACCORDING TO FORMAT 2 (IF OPT= 1, CALCULATES
14*  C       PARAMETERS AND COMPUTES THEORETICAL RESPONSE, IF OPT= 2, READS
15*  C       PARAMETERS AND PREDICTS THEORETICAL RESPONSE, IF OPT= 3, READS
16*  C       MASS OF ONE BAR, PENDULUS LENGTH, INITIAL DISPLACEMENT - USES
17*  C       SPRING CONSTANT AND VISCOUS DAMPING COEFFICIENT OF PREVIOUS
18*  C       DATA AND PREDICTS THEORETICAL RESPONSE) NEXT DATA DESCRIBED AT
19*  C       PARAGRAPH NUMBER (OPT + 2).
20*  C   3. MASS OF ONE BAR, BMASS, IN LBS-SEC**2/INCH, PENDULUS LENGTH,
21*  C       PL, INITIAL DISPLACEMENT, X0, FIRST REBOUND MAXIMUM DISPLACE-
22*  C       MENT, X1M, IN INCHES, DURATION OF CONTACT, TC, IN SECONDS,
23*  C       ACCORDING TO FORMAT 3
24*  C   4. MASS OF ONE BAR, PENDULUS LENGTH, INITIAL DISPLACEMENT AS IN 3,
25*  C       SPRING CONSTANT, PK, IN LBS/INCH, DAMPING CONSTANT, PC, IN
26*  C       LBS-SEC/INCH, ACCORDING TO FORMAT 3
27*  C   5. MASS OF ONE BAR, PENDULUS LENGTH, INITIAL DISPLACEMENT, AS IN 3
28*  C
29*  C
30*  C   INTEGER OPT
31*  C   DATA G/385.644/
32*  C   PI=3.14159
33*  C   1 FORMAT(I2,8X,I2,8X,I2)
34*  C   2 FORMAT(I1)
35*  C   3 FORMAT( )

```

```

36*      5 FORMAT(13X,I2,15X,E11.5,8X,E11.5)
37*      READ(5,1) ICASES,IBOUND,IPOINT
38*      DO 10000 I=1,ICASES,1
39*      READ(5,2) OPT
40*      IF (OPT.NE.1) GO TO 20
41*      READ(5,3) BMASS,PL,X0,X1M,TC
42*      EL=ALOG(((2.0*PL**2)/X0**2)*(1.0-COS(X1M/PL)))
43*      ZETA=SQRT(EL**2/(EL**2+4.0*PI**2))
44*      PK=BMASS*PI**2/(TC**2*(1.0-ZETA**2))
45*      PC= 2.0*ZETA*SQRT(PK*BMASS)
46*      TR=PI*SQRT(PL/G)
47*      WN=SQRT(PK/BMASS)
48*      WRITE(6,4) BMASS,PL,X0,X1M,TC,PK,PC,TR
49*      4 FORMAT(7X,56H*** IMPACTING KELVIN-VOIGT VISCOELASTIC PENDULI
50*      A***//13X,6HMASS= ,E11.5,8X,8HLENGTH= ,E11.5/18X,22HINITIAL DISPLAC
51*      BEMENT= ,E11.5//25X,20HMEASURED PARAMETERS/13X,6HXMAX= ,E11.5,16H
52*      C CONTACT TIME= ,E11.5//23X,24HKELVIN-VOIGT PARAMETERS/13X,3HK= ,
53*      DE11.5,16X,3HC= ,E11.5/22X,14HREBOUND TIME= ,E11.5//11X,7HREBOUND,
54*      E15X,4HTIME,12X,12HDISPLACEMENT/)
55*      GO TO 1000
56*      20 IF (OPT.EQ.2) READ(5,3) BMASS,PL,X0,PK,PC
57*      IF (OPT.EQ.3) READ(5,3) BMASS,PL,X0
58*      TR=PI*SQRT(PL/G)
59*      ZETA=PC/(2.0*SQRT(PK*BMASS))
60*      WN=SQRT(PK/BMASS)
61*      WD=WN*SQRT(1.0-ZETA**2)
62*      TC=PI/WD
63*      WRITE(6,6) BMASS,PL,X0,PK,PC,TC,TR
64*      6 FORMAT(7X,56H*** IMPACTING KELVIN-VOIGT VISCO-ELASTIC PENDULI
65*      A***//13X,6HMASS= ,E11.5,8X,8HLENGTH= ,E11.5/18X,22HINITIAL DISPLAC
66*      BEMENT= ,E11.5//23X,24HKELVIN-VOIGT PARAMETERS/13X,3HK= ,E11.5,16X
67*      C,3HC= ,E11.5/12X,4HTC= ,E11.5,15X,4HTR= ,E11.5//11X,7HREBOUND,15X,
68*      D4HTIME,12X,12HDISPLACEMENT/)
69*      01000 FWN=SQRT(G/PL)
70*      M=0
71*      T=0

```

```

72*      IPOI=(IPOINT+1)/2
73*      POINT=FLOAT(IPOINT)
74*      DO 09090 N=1,IPOI,1
75*      IF (N.EQ.1) GO TO 30
76*      T=T+TR/( POINT-1.0)
77*      30 X=X0*COS(FWN*T)
78*      IF (ABS(X).LE.1E-5) X=0.0
79*      09090 WRITE(6,5) M,T,X
80*      PHI=ATAN(ZETA/SQRT(1.0-ZETA**2))
81*      DK=-(ZETA*WN*TC)
82*      AMPL=1.0/SQRT(1.0-ZETA**2)
83*      DO 10000 J=1,IBOUND,1
84*      RJ=FLOAT(J)
85*      T=TR*(RJ-0.5)+RJ*TC
86*      DO 10000 K=1,IPOINT,1
87*      IF (K.EQ.1) GO TO 11111
88*      T=T+TR/(POINT-1.0)
89*      11111 X=AMPL*X0*(-1.0)**J*EXP(RJ*DK)*COS(RJ*PI+PHI)*SIN(FWN*(T-RJ*TC-(RJ
90*      A-0.5)*TR))
91*      IF (ABS(X).LE.1E-5) X=0.0
92*      WRITE(6,5) J,T,X
93*      10000 CONTINUE
94*      STOP
95*      END

```

END OF COMPILATION: NO DIAGNOSTICS.

APPENDIX F

ANALYSIS OF SUPPORT CABLE ORIGINATED FORCING FUNCTION

The unexpected nature of the impact response obtained in the experimental investigation cast doubt on the validity of the assumption that the penduli act as freely oscillating masses when out of contact. An effect which might explain both the rebound periods which were shorter than expected and the rebound displacements which exceeded those preceding them is the application of an additional forcing function to the equations of motion during rebound. A likely place to look for such a forcing function is in the support wires of the experimental device.

It is apparent that the sum of the vertical components of the tensions in the four support wires must always balance the weight of the pendulum mass. If upon impact the wires deflect due to their own inertia, the tension in them must increase so that the weight of the pendulum mass be balanced. The result is that a tangential forcing function varying at the vibrating frequency of the support wires is introduced into the rebound motion.

Figure 28 describes the nomenclature to be used in the following analysis. It is assumed that each wire supports exactly one quarter of the pendulum's weight.

Figure 29 is a normal view of the \bar{y} - z plane. Let $z(\bar{y}, t)$ denote the displacement at time t of the point (\bar{y}, z) away from the \bar{y} axis.

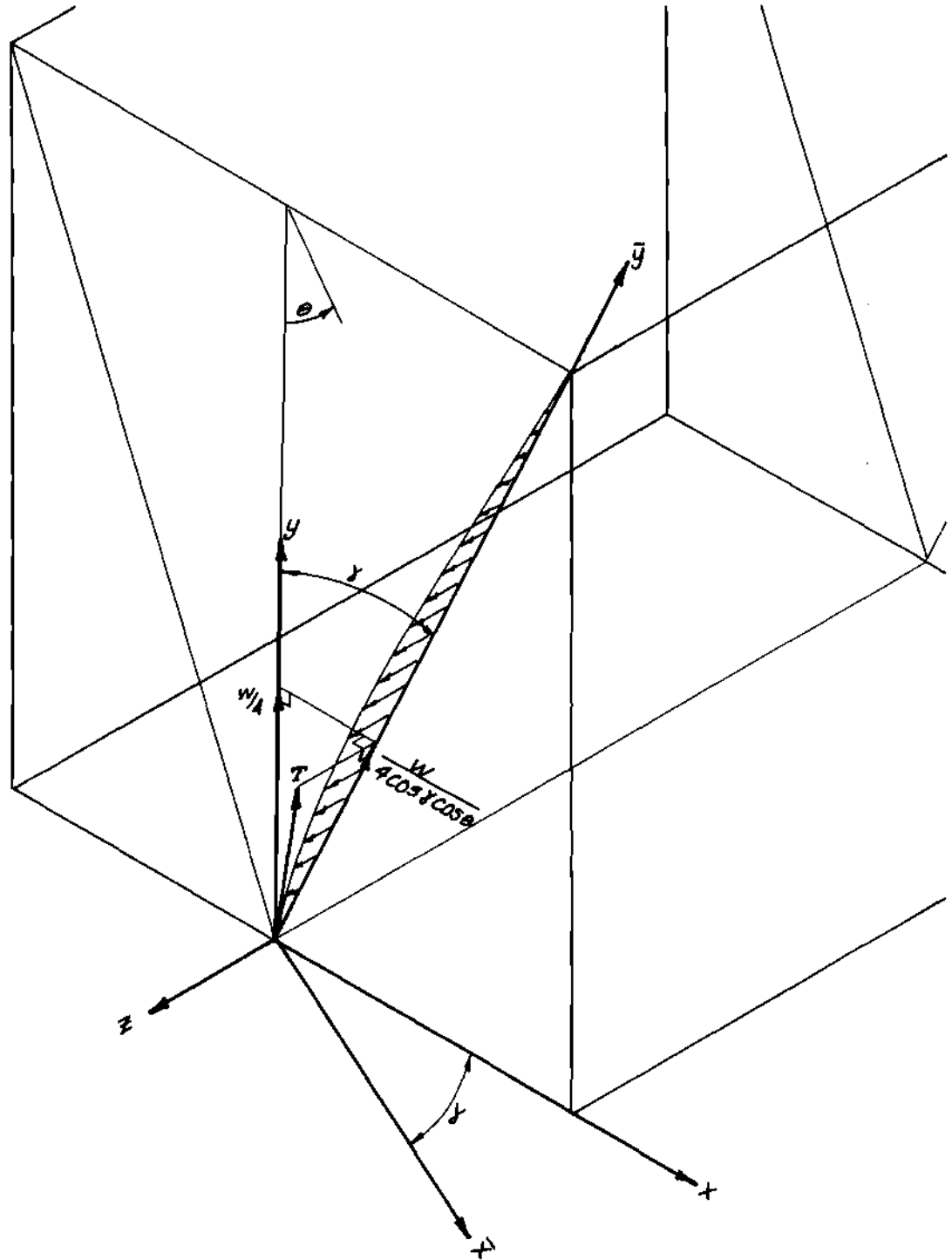


Figure 28. Support Wire Nomenclature

Assume the wire has zero resistance to bending and thus transmits only tensile force T . Also assume small displacements and slope α , so that $V = \text{constant}$ and $\Delta S = \Delta \bar{y}$.

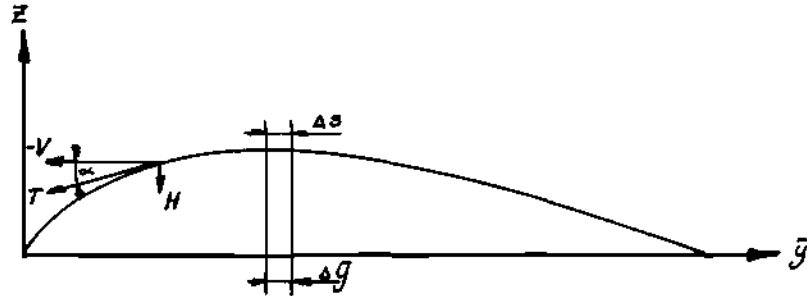


Figure 29. \bar{y} - z Plane

Note from the figure that

$$H(\bar{y}, t) = -V z_{\bar{y}}(\bar{y}, t) \quad *$$
(74)

Now since $\Delta S = \Delta \bar{y}$, the mass of element ΔS is given by

$$\rho \Delta \bar{y} \pi d^2/4 = \bar{\rho} \Delta \bar{y}$$
(75)

where d is the diameter of the wire, ρ is its mass density and $\bar{\rho}$ is its mass per unit length. Applying Newton's second law to an element yields

* Letter subscripts denote partial differentiation with respect to the subscripted variable, i.e. $z_{\bar{y}} \equiv \partial z / \partial \bar{y}$, $z_{tt} \equiv \partial^2 z / \partial t^2$, etc.

$$\bar{\rho} \Delta \bar{y} z_{tt}(\bar{y}, t) = -V z_g(\bar{y}, t) + V z_g(\bar{y} + \Delta \bar{y}, t) \quad (76)$$

or

$$z_{tt}(\bar{y}, t) = (V/\bar{\rho}) [z_g(\bar{y} + \Delta \bar{y}, t) - z_g(\bar{y}, t)] / \Delta \bar{y} \quad (77)$$

which, as $\Delta \bar{y}$ approaches zero, becomes

$$z_{tt}(\bar{y}, t) = (V/\bar{\rho}) z_{gg}(\bar{y}, t) \quad (78)$$

Letting $\sqrt{V/\bar{\rho}} = a$, this takes the form of the standard wave equation:

$$\partial^2 z / \partial t^2 = a^2 \partial^2 z / \partial \bar{y}^2 \quad (79)$$

Notice that it has been assumed that the chord length l remains constant. Measuring time from the moment of contact, the initial and boundary conditions are

$$z(0, t) = z(l, t) = 0 \quad (80)$$

$$z(\bar{y}, 0) = 0 \quad (81)$$

$$z_t(\bar{y}, 0) = (\dot{X}_0/l)(l - \bar{y}) \quad (82)$$

where \dot{x}_0 is the approaching velocity of the penduli as in the body of the thesis.

Let us assume a solution to equation 79 exists of the form

$$z(\bar{y}, t) = Y(\bar{y}) T(t) \quad (83)$$

implying

$$z_{tt} = Y(\bar{y}) T''(t) \quad (84)$$

and

$$z_{y\bar{y}} = Y''(\bar{y}) T(t) \quad (85)$$

Substitution of equations 84 and 85 into equation 79 yields

$$Y(\bar{y}) T''(t) = \alpha^2 Y''(\bar{y}) T(t) \quad (86)$$

which may be manipulated into the form

$$Y''(\bar{y})/Y(\bar{y}) = T''(t)/T(t) \alpha^2 = -\lambda \quad (87)$$

*Primes denote differentiation of single variable functions, i.e., $T' = dT/dt$, $T'' = d^2T/dt^2$, etc.

Equation 87 may be expressed as two independent equations with initial and boundary conditions:

$$Y''(\bar{y}) + \lambda Y(\bar{y}) = 0 \quad Y(0) = 0, \quad Y(l) = 0 \quad (88)$$

and

$$T''(t) + a^2 \lambda T(t) = 0 \quad T(0) = 0 \quad (89)$$

If λ is assumed positive, equation 88 may be shown to have the solution

$$Y(\bar{y}) = C_1 \sin(\bar{y}n\pi/l) \quad (90)$$

Under the same assumption equation 89 has a solution of the form

$$T(t) = C_2 \sin(tn\pi a/l) \quad (91)$$

Substituting equations 90 and 91 into equation 83, $z(\bar{y}, t)$ is found to be

$$z(\bar{y}, t) = C_3 \sin(\bar{y}n\pi/l) \sin(tn\pi a/l) \quad n = 1, 2, 3, \dots \quad (92)$$

and therefore by superposition

$$z(\bar{y}, t) = \sum_{n=1}^{\infty} A_n \sin(\bar{y} n \pi / l) \sin(t n \pi a / l) \quad (93)$$

Differentiating equation 93 once with respect to time yields

$$z_t(\bar{y}, t) = \sum_{n=1}^{\infty} A_n (n \pi a / l) \sin(\bar{y} n \pi / l) \cos(t n \pi a / l) \quad (94)$$

From equation 82

$$z_t(\bar{y}, 0) = \sum_{n=1}^{\infty} A_n (n \pi a / l) \sin(\bar{y} n \pi / l) = \dot{x}_0(l - \bar{y}) / l \quad (95)$$

The summation must be the Fourier series for the right-hand side of the equation on the interval $0 \leq \bar{y} \leq l$. This will be true if (9)

$$A_n n \pi a / l = b_n = (2/l) \int_0^l (\dot{x}_0 / l)(l - \bar{y}) \sin(\bar{y} n \pi / l) d\bar{y} \quad (96)$$

It is immediately seen that

$$A_n = b_n l / n \pi a \quad (97)$$

and upon integration equation 96 becomes

$$b_n = 2\dot{X}_0/n\pi \quad (98)$$

Thus the solution to equation 79 satisfying the conditions of equations 80, 81 and 82 is

$$x(\bar{y}, t) = (2\dot{X}_0 l / \pi^2 a) \sum_{n=1}^{\infty} (1/n^2) \sin(\bar{y}n\pi/l) \sin(tn\pi a/l) \quad (99)$$

By differentiation,

$$x_{\bar{y}}(\bar{y}, t) = (2\dot{X}_0 / \pi a) \sum_{n=1}^{\infty} (1/n) \cos(\bar{y}n\pi/l) \sin(tn\pi a/l) \quad (100)$$

Substituting equation 100 into equation 74 and evaluating at $\bar{y} = 0$ yields

$$H(0, t) = -(2\dot{X}_0 V / \pi a) \sum_{n=1}^{\infty} (1/n) \sin(tn\pi a/l) \quad (101)$$

Recalling that $a = \sqrt{V/\bar{\rho}}$, and noting from Figure 28 that

$$V = W/4 \cos \gamma \cos \theta \quad (102)$$

equation 101 becomes

$$H(0,t) = -(2\dot{X}_0/\pi)\sqrt{\rho W/4 \cos \gamma \cos \theta} \sum_{n=1}^{\infty} (1/n) \sin(tn\pi a/l) \quad (103)$$

Returning to the notation of Chapter II and assuming that for small θ the distortion of the $z\text{-}\bar{y}$ plane may be neglected, a horizontal forcing function

$$F = -(2\dot{X}_{N0}/\pi)\sqrt{\rho W/4 \cos \gamma \cos \theta} \sum_{n=1}^{\infty} (1/n) \sin(tn\pi a/l) \quad (104)$$

is applied to the pendulum by each support wire, where $t=0$ corresponds to the moment of contact. (A more elaborate investigation might take into account the delay involved between the time the strain wave stops the lower end of the first two support wires and when it reaches the second pair.) The tangential forcing function is given by $F \cos \theta$.

Summing forces in the tangential direction on a pendulum and recalling that $\dot{X}_0 = L\dot{\theta}_0$ yields, for small θ ,

$$\ddot{\theta} + g/L = -(\partial \dot{\theta}_{N0}/ML\pi)\sqrt{\rho W/4\cos Y} \sum_{n=1}^{\infty} (1/n) \sin(t n \pi a/l) \quad (105)$$

the modified equation of motion for the penduli. This equation is applicable from the moment of contact and therefore it must be superimposed on the contact equations given by the rheological models as well as being used to describe rebound motion. It is hypothesized that the effect of damping on the forcing function of equation 105 can result in either positive or negative net additional restoring impulse to the penduli for different impact velocities, and that the application of such impulses could produce the response obtained experimentally. The convergence of partial sums of equation 105 has not been investigated; however the convergence of equation 99, from which equation 105 was derived, is known to be both uniform and absolute (10,11).

BIBLIOGRAPHY

1. W. Goldsmith, *Impact: the Theory and Physical Behaviour of Colliding Solids*, E. Arnold and Co., London, 1960.
2. K. W. Maier, "Equations and Charts for Analyzing Impact Between Masses," *Product Engineering*, April 29, 1962.
3. C. M. Zener, *Elasticity and Anelasticity of Metals*, University of Chicago Press, 1948.
4. N. H. Polakowski and E. J. Ripling, *Strength and Structure of Engineering Materials*, Prentice-Hall, 1966.
5. G. S. Pisarenko, *Dissipation of Energy During Mechanical Vibration*, Akademiyanauk Ukraniskoi SSR, 1962--trans. National Lending Library for Science and Technology, Boston Spa, London, 1964.
6. R. V. Churchill, *Operational Mathematics*, McGraw-Hill, 1958.
7. R. C. Weast and S. M. Selby eds., *Handbook of Mathematical Tables*, The Chemical Rubber Co., 1964.
8. H. C. Roters, *Electromagnetic Devices*, John Wiley and Sons, 1941.
9. R. V. Churchill, *Fourier Series and Boundary Value Problems*, McGraw-Hill, 1963.
10. D. V. Widder, *Advanced Calculus*, Prentice-Hall, 1961.
11. E. Kreyszig, *Advanced Engineering Mathematics*, John Wiley and Sons, 1962.
12. W. T. Thomson, *Vibration Theory and Applications*, Prentice-Hall, 1965.
13. F. S. Tse, I. E. Morse and R. T. Hinkle, *Mechanical Vibrations*, Allyn and Bacon, Inc., 1963.
14. R. L. Wirth, "Analysis of a High-Speed Solenoid-Actuated Mechanism," *Journal of Engineering for Industry*, A.S.M.E., August, 1968.